JOURNAL OF GEOPHYSICAL RESEARCH: EARTH SURFACE, VOL. 118, 1400–1419, doi:10.1002/jgrf.20102, 2013

Discrimination of bed form scales using robust spline filters and wavelet transforms: Methods and application to synthetic signals and bed forms of the Río Paraná, Argentina

Ronald R. Gutierrez,[1] Jorge D. Abad,[1] Daniel R. Parsons,[2] and James L. Best[3]

Received 7 April 2012; revised 28 June 2013; accepted 4 July 2013; published 12 August 2013.

[1] There is no standard nomenclature and procedure to systematically identify the scale and magnitude of bed forms such as bars, dunes, and ripples that are commonly present in many sedimentary environments. This paper proposes a standardization of the nomenclature and symbolic representation of bed forms and details the combined application of robust spline filters and continuous wavelet transforms to discriminate these morphodynamic features, allowing the quantitative recognition of bed form hierarchies. Herein the proposed methodology for bed form discrimination is first applied to synthetic bed form profiles, which are sampled at a Nyquist ratio interval of 2.5–50 and a signal-to-noise ratio interval of 1–20 and subsequently applied to a detailed 3-D bed topography from the Río Paraná, Argentina, which exhibits large-scale dunes with superimposed, smaller bed forms. After discriminating the synthetic bed form signals into three-bed form hierarchies that represent bars, dunes, and ripples, the accuracy of the methodology is quantified by estimating the reproducibility, the cross correlation, and the standard deviation ratio of the actual and retrieved signals. For the case of the field measurements, the proposed method is used to discriminate small and large dunes and subsequently obtain and statistically analyze the common morphological descriptors such as wavelength, slope, and amplitude of both stoss and lee sides of these different size bed forms. Analysis of the synthetic signals demonstrates that the Morlet wavelet function is the most efficient in retrieving smaller periodicities such as ripples and smaller dunes and that the proposed methodology effectively discriminates waves of different periods for Nyquist ratios higher than 25 and signal-to-noise ratios higher than 5. The analysis of bed forms in the Río Paraná reveals that, in most cases, a Gamma probability distribution, with a positive skewness, best describes the dimensionless wavelength and amplitude for both the lee and stoss sides of large dunes. For the case of smaller superimposed dunes, the dimensionless wavelength shows a discrete behavior that is governed by the sampling frequency of the data, and the dimensionless amplitude better fits the Gamma probability distribution, again with a positive skewness. This paper thus provides a robust methodology for systematically identifying the scales and magnitudes of bed forms in a range of environments.

Citation: Gutierrez, R. R., J. D. Abad, D. R. Parsons, and J. L. Best (2013), Discrimination of bed form scales using robust spline filters and wavelet transforms: Methods and application to synthetic signals and bed forms of the Río Paraná, Argentina, *J. Geophys. Res. Earth Surf.*, *118*, 1400–1418, doi:10.1002/jgrf.20102.

1. Introduction

[2] The quantification of variability in bed form geometry is necessary for many scientific and practical applications, such as in quantifying and explaining: (1) bed roughness [*Tuijnder and Ribberink*, 2009; *Aberle et al.*, 2010], (2) the formation of cross-strata [*Prave and Duke*, 1990; *Paola and Borgman*, 1991; *Storms et al.*, 1999; *Longhitano and Nemec*, 2005; *Blom and Kleinhans*, 2007; *Ghiene et al.*, 2010; *Quin*, 2011; *Reesink and Bridge*, 2011], (3) the vertical sorting of sediments [*Kleinhans*, 2004; *Blom and Parker*, 2004; *Kleinhans*, 2005; *Kuhnle et al.*, 2006], (4) sediment

[1]Department of Civil and Environmental Engineering, University of Pittsburgh, Pittsburgh, Pennsylvania, USA.
[2]School of Geography, University of Hull, Kingston upon Hull, UK.
[3]Departments of Geology, Geography and Geographic Information Science, Mechanical Science and Engineering, and Ven Te Chow Hydrosystems Laboratory, University of Illinois at Urbana-Champaign, Urbana, Illinois, USA.

Corresponding author: J. D. Abad, Department of Civil and Environmental Engineering, University of Pittsburgh, Benedum Engineering Hall, Pittsburgh, PA 15261, USA. (jabad@pitt.edu)

2169-9003/13/10.1002/jgrf.20102

transport rates [*Haque and Mahmood*, 1987; *Wilbers and Brinke*, 2003; *Elhakeem and Imran*, 2006; *Kostaschuk*, 2006; *Frings and Kleinhans*, 2008; *Singh et al.*, 2009], (5) the transition between 2-D and 3-D dunes [*Venditti et al.*, 2005], and (6) velocity pulsations within the flow [*Haque and Mahmood*, 1986; *Holmes and Garcia*, 2008; *Shugar et al.*, 2010]. Such quantification is also required for the numerical modeling of flow over bed forms (e.g., [*Keylock et al.*, 2005; *Wang and Cheng*, 2006; *Stoesser et al.*, 2008]), assessing the interaction between flow over bed forms and groundwater [*Cardenas et al.*, 2004; *Cardenas and Wilson*, 2006; *Cardenas et al.*, 2007], and evaluating contaminant transport [*Packman et al.*, 2004]. For practical purposes, the study of the variability of bed forms is important in the following: (1) the prediction of floods and flow resistance [*Annambhotla et al.*, 1972; *Julien and Klaasen*, 1995; *Prent and Hickin*, 2002; *Kheiashy et al.*, 2007; *Kaufmann et al.*, 2008; *Warmink et al.*, 2010], (2) the prediction of potential disturbance to man-made structures, such as river tunnels [*Amsler and Garcia*, 1997] and bridges, (3) predicting future changes in sediment transport rates and biotic responses following dam removal [e.g., *Morley et al.*, 2008], (4) estimating the relationship between bed form characteristics and biota [*Wildhaber et al.*, 2003; *Takeda et al.*, 2001], and (5) planning river restoration projects [e.g., *Jacobson and Galat*, 2006].

[3] The morphology and dynamics of alluvial bed forms are strongly governed by the inter-relationship between sediment transport and the hydraulic conditions. The persistent variability in the geometry and migration rates of bed forms is the hallmark of behavior under, and interacting with, unidirectional shear flows [*Jerolmack and Mohrig*, 2005]. However, at present we lack a consistent, nonarbitrary, quantitative description of both the morphology and dynamics of bed forms across a range of spatial scales that is necessary to understand the effect of their morphology upon bed form migration, sediment transport, and the resultant bed roughness.

[4] Theoretical research on the morphodynamics of noncohesive channel beds has largely followed five distinctive approaches [*Haque and Mahmood*, 1985] in which sediment continuity was incorporated into the governing equations [*Exner*, 1925], the water-bed interface was regarded as a Kelvin-Helmholtz instability [*Liu*, 1957], the fluid-bed interface was investigated using linear stability theory [*Kennedy*, 1963], kinematically admissible bed form profiles were obtained using the Helmholtz-Kirchoff method [*Mercer*, 1971], and dimensionless statistical correlations were performed [*Yalin*, 1964]. Statistical methods developed for the description of bed forms in alluvial channels were first proposed by *Nordin and Algert* [1966] and *Engelund and Fredsøe* [1982]. Research performed following the fifth statistical approach has typically used morphometric parameters such as bed form height (Δ), wavelength (λ), and steepness (Δ/λ) to describe and classify features such as ripples and dunes commonly found on continental shelves and within river channels in various superimposed states [*Ashley*, 1990; *Catano-Lopera et al.*, 2009].

[5] Some early studies considered bed form profiles to be stochastic variables [*Nordin*, 1971; *Jain and Kennedy*, 1971; *Moll et al.*, 1987] that were analyzed by using time series analysis techniques [*Levey et al.*, 1980]. However,

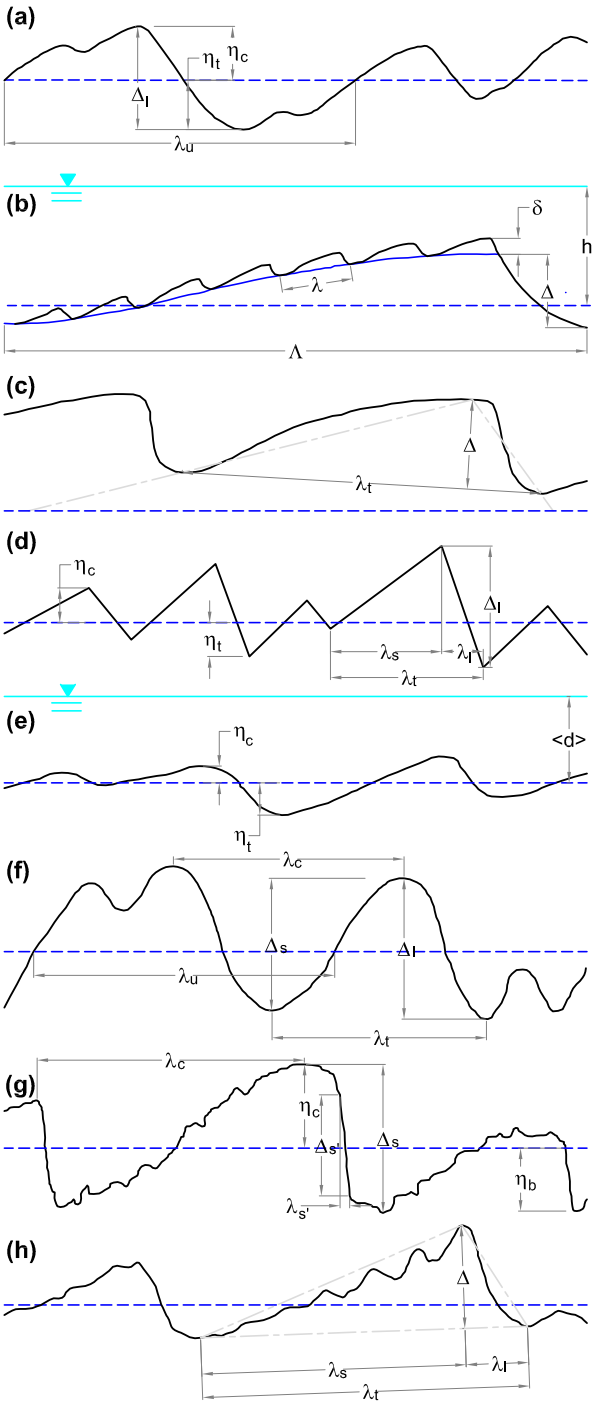

Figure 1. Bed form parameters after (a) *Annambhotla et al.* [1972], (b) *Yalin and Lai* [1985] (c) *Wilbers and Brinke* [2003], (d) *van der Mark et al.* [2006], (e) *Jerolmack and Mohrig* [2005], (f) *van der Mark and Blom* [2007], (f) *van der Mark et al.* [2008b], and (h) *Knaapen* [2008]. In each case, the blue dotted lines represent the mean bed elevation.

more recent studies have used spatial scaling techniques that treat bed elevations in a bed form profile as a random function, rather than identifying individual bed forms in a profile [*Nikora et al.*, 1997; *Jerolmack and Mohrig*, 2005; *van der Mark et al.*, 2008a].

[6] There is laboratory and field evidence that both the variability of bed form morphology and the variability in the geometric descriptors (e.g., steepness) of individual bed forms within a given reach affect the reach-averaged form roughness [*Simons and Richardson*, 1962; *Yalin and Lai*, 1985; *Yang et al.*, 2005; *van der Mark et al.*, 2008a; *Dimas and Kolokythas*, 2011; *Kumar*, 2011]). Based on experimental measurements and field data, *Yalin and Lai* [1985] proposed that the form resistance, f'', when ripples are superimposed upon dunes can be estimated as $f'' = 4\Xi$ if $\Xi > \simeq 10^{-2}$, and as $f'' = [3.3\log(\Xi - 1) - 2.3]^{-2}$ if $\Xi < \simeq 10^{-2}$; where $\Xi = \frac{\Delta^2}{\Lambda h}$, Δ and Λ are respectively the amplitude and wavelength of the dunes, and h is the water depth (see Figure 1b for the geometric definition of these variables). These relationships suggest that drag resistance is dependent mainly on the geometric characteristics of dunes. Field measurements also prove the importance of the geometry of larger dunes in the drag resistance, even using other relationships such as those proposed by Vanoni-Hwang, van Rijn (modified) and Engelund as reported by *Julien et al.* [2002]. Moreover, *van der Mark et al.* [2008a] hypothesized that the variability of individual bed forms within a reach affects the reach-averaged form roughness and based this hypothesis on the analogy between grain roughness and form roughness. For example, the 65%, 84%, or 90% percentiles of the grain size distribution are often used as a representative particle diameter in predicting the grain roughness. Similarly, form roughness may also be determined from bed forms that are higher, longer, or steeper than the median or mean bed form height, bed form length, or bed form steepness, respectively [*van der Mark et al.*, 2008a].

[7] Past approaches to the quantification of bed form variability have used and applied spectral analysis [*Hino*, 1968; *Jain and Kennedy*, 1971, 1974; *Annambhotla et al.*, 1972; *Levey et al.*, 1980; *Kheiashy et al.*, 2007], smoothing techniques such as a moving average [*Brinke et al.*, 1999; *Julien et al.*, 2002; *Wilbers and Brinke*, 2003; *Hoekstra et al.*, 2004; *Frings and Kleinhans*, 2008; *van der Mark et al.*, 2008a], signal roughness techniques [*Singh et al.*, 2009], fractals [*Wildhaber et al.*, 2003], and logistic regression [*Karbasi et al.*, 2010]. However, past research concerning the analysis of time series exhibiting multiscale time variability (similar to the multiscale spatial variability of bed form features) using moving average techniques, as well as Fourier series analysis, has generally shown that these techniques are insufficient as a tool to extract the long-term variation from signals that contain a long-term trend with a superimposed fine oscillation (i.e., the short term variation) [*Takezawa*, 2006]. This lack of success is primarily because when using spectral analysis, the major assumption is that the bed form waves are two-dimensional and not highly variable in the cross-stream direction [*Levey et al.*, 1980]. Likewise, the Fourier transform, which is used in spectral analysis, has severe limitations when analyzing signals that include significant departures from stationarity and consist of intermittent and/or aperiodic processes. In these cases, a high number of Fourier coefficients are necessary to take these processes into account, that may be visible in some intervals but not in others [*Labat*, 2005]. Thus, a limited representation of the frequencies of nonlinear processes, such as river bed morphology, is obtained.

[8] Wavelet transforms were developed to overcome the limitations of Fourier transforms and have been applied to fluid mechanics in the isolation of coherent structures in turbulent flows [*Farge*, 1992], in analyzing the temporal variability of coherent convective storm structures [*Kumar and Foufoula-Georgiou*, 1993], within investigation of long-term land temperature/climate series [*Baulinas*, 1997], in analyzing oxygen isotopic ratios from marine sediments [*Prokoph and Veizer*, 1999], and in analyzing the local curvature of meanders [*Abad*, 2009]. Some recent applications of 1-D wavelets in sedimentology encompass temporal variations within streamflow and sediment loads [*Rossi et al.*, 2009], characterization of bed form morphology [*Catano-Lopera et al.*, 2009; *Singh et al.*, 2011], sediment concentration distributions [*Felix et al.*, 2005], the recognition of patterns in seabed morphology [*Little*, 1994], analysis of riverbed roughness [*Nyander et al.*, 2003], and investigation of flow structure over alluvial sand dunes [*Shugar et al.*, 2010]. Herein we demonstrate that this technique identifies the various scales of bed forms present within a series and significantly improves the quantification of form roughness at different bed form scales.

2. Bed Form Discrimination Method and Field Study Site

2.1. Data

2.1.1. Synthetic Signal Data

[9] In order to assess the accuracy of the discrimination methodology proposed herein, a set of well-constrained synthetic signals were first examined. These signals comprise three waves of different periodicity that are intended to replicate ripples, dunes, and bars. Ripples ($\eta_{1,3}$) are represented by a random signal generated using the Wichman-Hill algorithm that in some instances imposes periods not sufficiently large on the generated signals [*Kroesse et al.*, 2011]. The mean of these signals is equal to zero, and their variance was changed in order to obtain an interval with signal-to-noise ratios (SNR) from approximately 1 to 20. The SNR is defined as the ratio between the variance of the random signal and the variance of the signal comprised by the summation of the bar and dune signals.

[10] The stoss side of the dunes is represented by the lower-regime dune equation $\eta^s_{2,3}(x)$ (equation (1)) proposed by *Haque and Mahmood* [1985]. The lee face is represented by a straight line with slope $S^l_{2,3}$, defined by equation (2).

$$\eta^s_{2,3} = S^s_{2,3}\lambda_{2,3}\left\{\frac{1}{2\pi\sin\frac{k\pi}{2}}\left(\ln\sin\frac{\pi}{\lambda_{2,3}}\left(x+\frac{\lambda_{2,3}}{2}[1-k]\right) - \ln\sin\frac{\pi}{2}[1-k]\right)+\frac{x}{\lambda_{2,3}}\right\};\ \text{for } 0 \le x \le k\lambda_{2,3} \quad (1)$$

$$\eta^l_{2,3} = -\frac{S^l_{2,3}(\lambda_{2,3}-x)}{(k-1)\lambda_{2,3}};\ \text{ for } k\lambda_{2,3} < x \le \lambda_{2,3} \quad (2)$$

where x is the relative distance in meters; the dune stoss slope, $S^s_{2,3} = \tan(\theta)$, is defined for $\theta = 10°$ (see *Haque and Mahmood* [1985] for geometric details); $\lambda_{2,3}$ is the dune

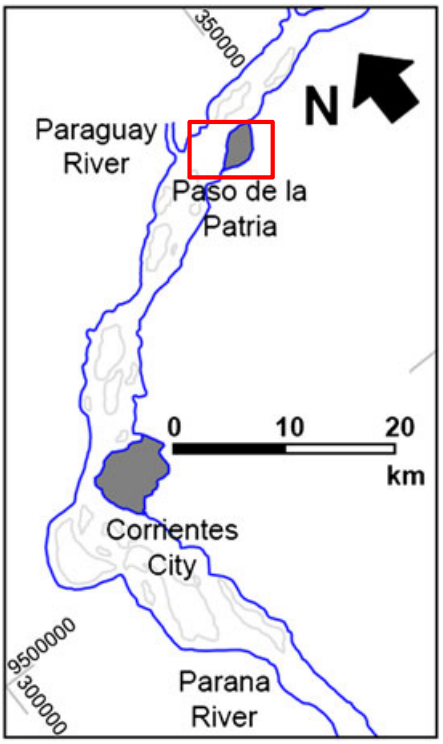

Figure 2. Location of the field site in the Río Paraná. The outlines of the islands are represented by thin gray lines.

wavelength (assumed to be equal to 10 m); and k is the normalized length of the stoss face, which was assumed to be equal to 0.7. This value is close to $k = 0.667$ as predicted by theory for mature ripples and dunes [*Haque and Mahmood*, 1985]. Centered (zero mean) versions of these dunes are used in the present application. Higher noise was applied to the dune stoss side than the lee side, in order to replicate the position of the ripples that are far more commonly superimposed on the stoss side of dunes.

[11] Bars are represented by the sinusoidal function $\eta_{3,3} = \Delta_{3,3} \times \sin(2\pi x/\lambda_{3,3} - \phi) + S_b$; where $\Delta_{3,3} = 0.05$ m is the amplitude, $\lambda_{3,3} = 200$ m is the wavelength, $\phi = 100$ is the phase and $S_b = 0.05x$. The term S_b provides a slope in this synthetic bar signal.

[12] The bed form synthetic signals are discretized at sampling intervals $\Delta x = 2$, 1, 0.5, 0.167, 0.125 m, and 0.1 m. Based on the ratio proposed by *Das et al.* [2008], the Nyquist ratio (NR) is defined as the number of times (> 1) the Nyquist sample rate is necessary to accurately recover the intermediate bed form scales (e.g., dunes).

[13] Since the life span of bed forms depends on the sediment transport rate that is fixed by flow conditions and the bed form excursion, defined as the distance over which an individual bed form may travel [*Allen*, 1982], the Nyquist sample rate aims to estimate the best sampling intervals for bed forms where the intermediate scales present longer life spans than that of the shorter scales (e.g., ripples). Since the Nyquist rate to recover dunes of $\lambda_{2,3} = 10$ m is $\Delta x_N = 5$ m, an interval of NR = $\Delta x_N/\Delta x$ of 2.5, 5, 10, 30, 40, and 50 is obtained.

[14] Additionally, synthetic bed form data exhibiting self-similarity characteristics were generated. Such data are comprised by the following: (1) the same synthetic ripples described above; (2) small and medium dunes (described by equations (1) and (2), whose amplitude follows the Gamma distribution as determined by past studies [e.g., *Paola and Borgman*, 1991; *Leclair et al.*, 1997], and whose wavelength and amplitude are related by the relationships described by *Jerolmack et al.* [2006]; and (3) sinusoidal bars (similar to those described above). The signals were also sampled at the same NR ranges described above.

2.1.2. Río Paraná Study Reach

[15] Bed forms measured within the Río Paraná, the world's seventh largest river by mean flow discharge [*Gupta*, 2007], are used as field test data herein. The study reach is located 16 km north of Corrientes, NE Argentina (see Figure 2), close to its confluence with the Río Paraguay.

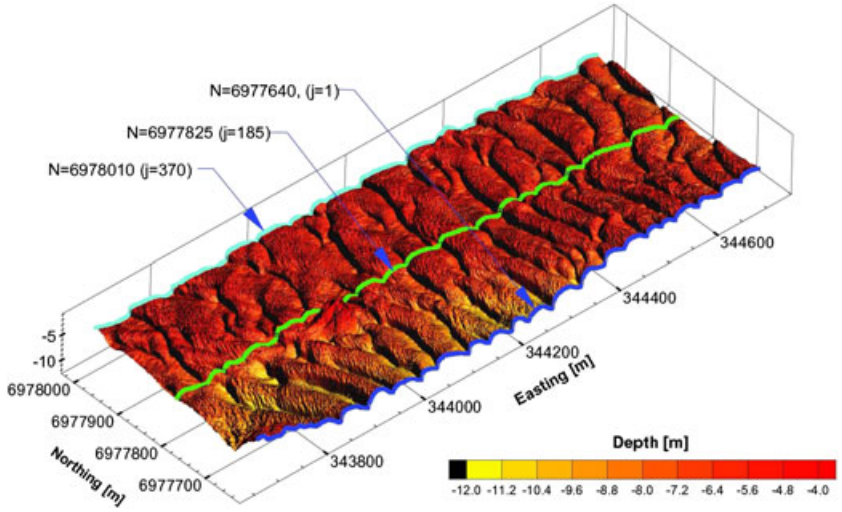

Figure 3. Bed morphology of the Río Paraná (after *Parsons et al.* [2005]). Flow is from right to left. The bed morphology shown here was measured in 2004 using a multibeam echo sounder. Note the ubiquitous superimposition of three-dimensional small dunes on larger three-dimensional dunes. The cyan, green, and blue lines represent the location of the profiles shown in Figure 4.

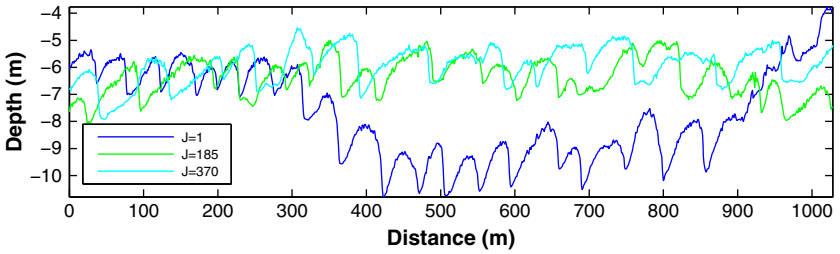

Figure 4. Bed form profiles in the Río Paraná (refer to sections j = 1, j = 185, and j = 370 in Figure 3). Flow is from left to right. Notice the existence of crestal platforms on dunes in the shallower flows.

[16] The flow regime of the Río Paraná is characterized by summer floods between February and March and spring low water levels [*Orfeo and Stevaux*, 2002]. At the study reach, the channel pattern can be classified as multi thread/braided [*Orfeo and Stevaux*, 2002] and the river is approximately 2.5 km wide and 5–12 m deep [*Parsons et al.*, 2005]. *Parsons et al.* [2005] surveyed a river bed 370 m wide, 1.2 km long, and 5–12 m deep using a RESON 8125 multibeam echo sounder and simultaneously obtained 3-D flow information using an acoustic Doppler current profiler. In order to prepare the data for the present analysis, a structured 1 m grid was obtained from this survey. Thus, 370 longitudinal transects of 1028 points (1 m sampling interval and NR = 100) were obtained. The first transect (j = 1) was located at the northing 6977640 and the last (j = 370) at the northing 6978010 (Figure 3). Figure 3 also shows that the bed morphology of the Río Paraná is characterized by 3-D dunes with few straight crests that are subparallel, but with numerous undulating crests that possess saddles and lobes that occasionally bifurcate, especially in regions of deeper flow [*Parsons et al.*, 2005]. Inspection of the transects at the center and boundaries of the survey area (Figure 4) shows that most of the dunes are highly asymmetric, with crestal platforms followed by marked changes of slope on the lee side (see *Parsons et al.* [2005] for more details). The larger bar feature is likely a forced bar created as flow is routed around a midchannel bar to the north of the field survey area.

2.2. The Hierarchical Scale Discrimination of Bed Forms

[17] There is currently no standard definition or methodology for the identification and discrimination of different bed form hierarchies (e.g., ripples, dunes, bars) generated on a natural mobile bed. As illustrated in Figure 1, various researchers have followed different approaches to quantifying and naming the geometric characteristics of bed forms. For example, bed form length has been defined as (i) the length of a line connecting two subsequent troughs, (ii) the distance between two successive mean bed level upcrossings (points that reach the mean bed elevation by describing a positive slope), (iii) the distance between two successive mean downcrossings (points that reach the mean bed elevation by describing a negative slope), and (iv) the distance of two successive crests or two successive troughs (see Figures 1c, 1f and 1h). Similarly, bed form height has been defined as either the difference in elevation between a crest and its downstream trough, or as the shortest distance between a crestal elevation and the line between two troughs [*van der Mark and Blom*, 2007]. Likewise, some researchers (Figures 1d and 1f) have discriminated the length and amplitude of both the lee and stoss sides of dunes, which is necessary because they represent markedly different regions of flow over asymmetrical dunes. In the lee side, a region of flow separation, with reattachment occurring approximately 4–8 dune heights downstream of the crest and an expanding flow region are formed [*Best*, 2005; *Shugar et al.*, 2010]. These same gross patterns of flow also exist over the stoss and lee sides of the ripples, although dunes influence the water surface elevation and generate large-scale macro turbulence that may reach the water surface [*Kostaschuk and Church*, 1993; *Bennett and Best*, 1996; *Best*, 2005; *Robert and Uhlman*, 2001].

[18] Scaling remains a characteristic signature of bed forms [*Aberle et al.*, 2010], and both field and laboratory data often show multiple superimposed scales of bed forms. It is therefore frequently necessary to effectively subdivide

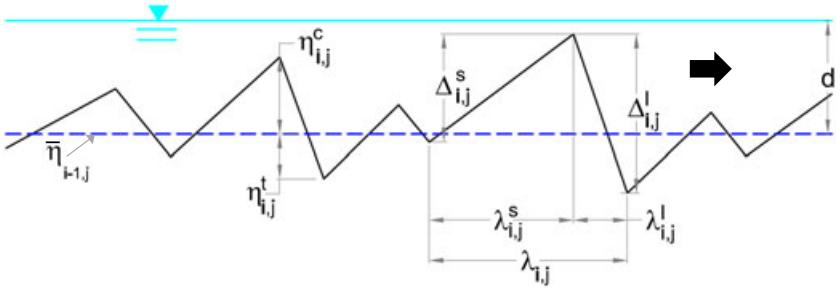

Figure 5. Symbolic representation of bed form descriptors for a given hierarchy adopted in the present paper. These descriptors mainly agree with those presented by *van der Mark et al.* [2006], but are applied on all of the bed form hierarchies. The bold black arrow represents the flow orientation and the blue dashed line the mean bed elevation of the preceding bed form scale.

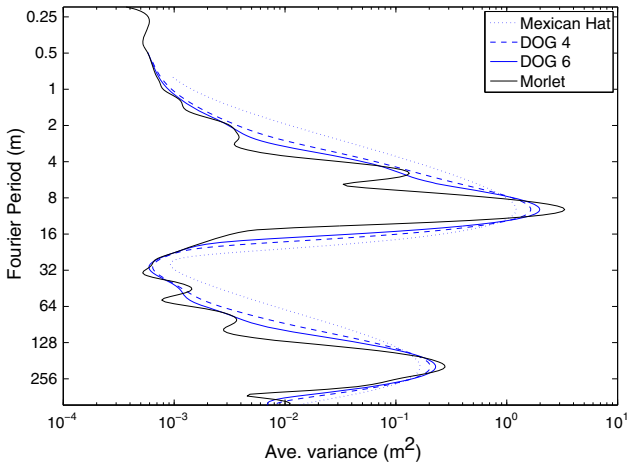

Figure 6. Wavelet global spectrum for Morlet and the derivatives of the Gaussian wavelet functions for signal SSNR100SNR494. The former retrieves higher frequencies such as the synthetic ripples with ∼0.30 m of wavelength, at any signal-to-noise ratio and Nyquist ratio. It is important to note that the 5 m wavelength is imposed by the synthetic ripples.

these differing bed form scales into useful, quantified waveforms with different periodicities. Several experiments indicate that ripple heights and wavelengths are independent of the flow depth [*Richards*, 1980; *Engelund and Fredsøe*, 1982; *Baas*, 1999; *Raudkivi*, 1997; *Coleman and Eling*, 2000; *Charru and Hinch*, 2006; *Colombini and Stocchino*, 2011; *Coleman and Nikora*, 2011]; furthermore, the equilibrium ripple height is remarkably independent of the grain size [*Raudkivi*, 1997]. *Ashley* [1990] proposed arbitrary thresholds of 5, 10, and 100 m for bed form length to differentiate "small", "medium" and "large" dunes and proposed a classification scheme to distinguish ripples from dunes by defining ripples as features that have wavelengths generally less than 0.6 m. Although this criterion is based on an observational gap (which is currently being filled), it is often used as an accepted criterion for distinguishing between ripples and dunes but without any theoretical or causative process explanation. In practice, the discrimination between ripples and dunes is often taken as obvious, so that many authors fail to explain the criteria used for their discrimination in field and laboratory studies [*Jerolmack et al.*, 2006]. It is thus clear that the study of differing scales of bed forms requires both a standardized method for their quantification and description of their geometric descriptors.

[19] The most widely used definitions of various bed form geometric descriptors are given in Figures 1a, 1b, 1d, 1e and 1f, with the definitions in Figures 1c and 1h often not being used [*van der Mark et al.*, 2006]. In order to standardize the symbolic representation of bed form geometric descriptors in bed form hierarchies, the symbols presented in Figure 5 are adopted herein. These symbols mainly agree with those presented by *van der Mark et al.* [2006], as applied to all bed form hierarchies and has been widely used in past research, although not on a standardized basis (see Figure 1). Each descriptor is represented by a letter, e.g., η (bed form elevation), λ (bed form length), Δ (for bed form height), and h (for water depth) followed by three indicators that represent (1) its position (as a superscript, but avoiding this descriptor if the bed form elevation is represented), e.g., crest (c), trough (b), stoss (s), and lee (l); (2) its ordinal with respect to all the hierarchies (as subscript and giving the first ordinal to the higher frequencies; e.g., ripples or small dunes); and (3) the total number of hierarchies (as a subscript). Therefore, the first hierarchy corresponds to ripples (or small dunes), the second to dunes, and the third to bars. Thus, for h (or η) the following relationship is always verified: $h = h_{1,3} + h_{2,3} + h_{3,3}$.

2.3. Method of Bed Form Scale Discrimination

[20] Investigations on bed form dynamics face the difficulty of defining an objective methodology to adequately quantify bed forms of different scale. This difficulty is principally due to the deterministic and stochastic nature of bed forms, where bed form profiles (BFPs) can further be viewed as a series of discrete bed form elements, continuous bed elevation fields, or some combination of these perspectives [*Coleman and Nikora*, 2011]. *van der Mark et al.* [2006] proposed a methodology, named the bed form tracking tool, which uses spectral analysis and a weighted moving average as a smoothing technique over BFPs that were previously verified to be statistically homogeneous. Generally speaking, such a methodology works according to the following procedure over individual BFPs: (1) it finds and replaces outliers, (2) a trend line is estimated based on the nature of the BFP (e.g., flume experiments or field measurements), (3) the BFP is detrended, (4) the BFP is filtered by applying a weighted moving average filter, (5) the zero upcrossings (points where the filtered BFP crosses the zero line in an upward direction) and downcrossings (points where the filtered BFP crosses the zero line in a downward direction; Figure 1g) are obtained, and finally (6) the geometric characteristics of the individual bed forms are estimated. This methodology performs reasonably well in minimizing any subjectivity in the estimation of the variability of bed forms, although it uses a filter that may not be completely suitable to detrend a BFP. A weighted average is any average that has multiplying factors to give different weights to data at different positions in the sample window. Mathematically, the moving average is a convolution of the data points with a fixed weighting function, and can therefore be considered as a rigid convolution function. The present work proposes the use of robust spline filters and the application of continuous wavelet transforms to perform a hierarchical discrimination and separation of different bed form scales. Discrete wavelet transforms and robust spline filters have been successfully used in the discrimination of engineering surfaces [*Raja et al.*, 2002], which, similar to bed forms, are comprised of a range of spatial wavelengths. Engineering surfaces are split into form profiles that are similar to bars, waviness profiles that are similar to dunes and roughness profiles that are similar to ripples [*Raja et al.*, 2002].

2.3.1. The Robust Spline Filter and the Wavelet Transform

[21] A fully automated robust spline procedure for uniformly sampled data sets is used herein. The algorithm, based on a penalized least squares method, allows fast smoothing of uniformly sampled data by means of the

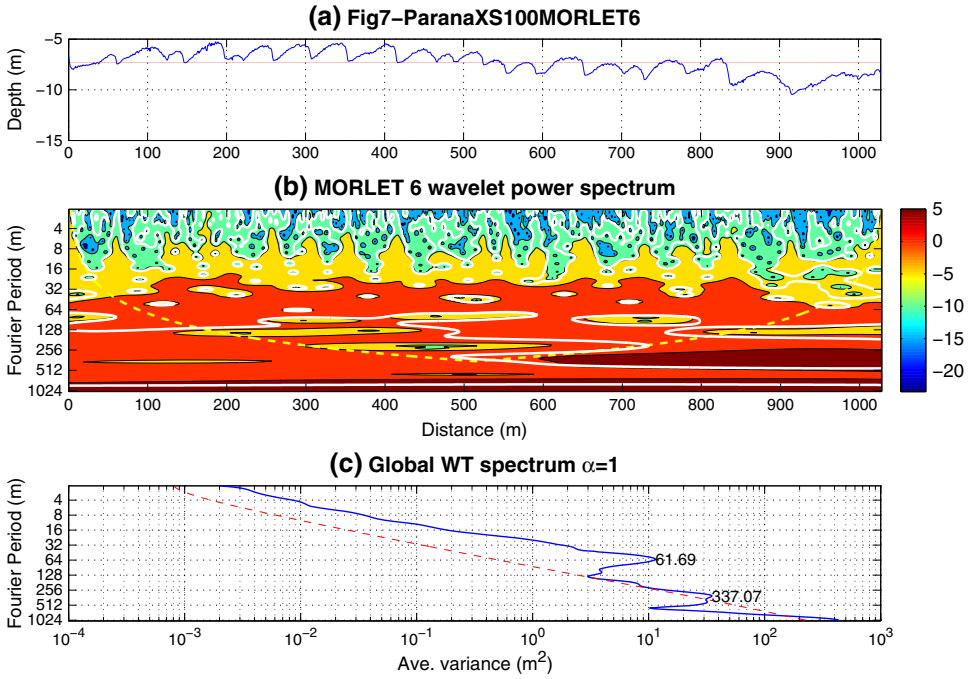

Figure 7. Wavelet analysis output for section j = 100. Bed form migration from left to right. (a) Bed form profile at section j = 100, (b) contours of the wavelet power spectrum using the Morlet wavelet function (dotted yellow line represents the cone of influence and the bold contours are the contours at 95% confidence limits), and (c) global wavelet power spectrum showing the main frequencies in section j = 100 (the dotted red line represents the 95% confidence interval; thus, the peaks located at the right side of the red line are the wavelengths at 95% of the confidence level). The higher frequency, 337 m, is used to discriminate the third bed form hierarchy (bars).

discrete cosine transform. To minimize or cancel the side effects of high leverage, the algorithm constructs weights with a specified weighting function by using the current residuals and updating them, from iteration to iteration, until the residuals remain unchanged [*Garcia*, 2010]. The smoothed data is estimated by the parameter s, which is a real positive scalar that controls the degree of smoothing.

[22] Wavelets have advantages over traditional Fourier methods in analyzing physical situations where the signal contains discontinuities and sharp spikes. They also provide a flexible time or spatial-scale window that is localized on temporal or spatial-scale planes [*Raja et al.*, 2002]. The most widely used continuous wavelet functions are the Morlet and nth derivatives of the Gaussian. Among the latter, the Ricker or so-called Mexican hat wavelet represents the second derivative. The selection of the appropriate wavelet function depends on both the mathematical and physical nature of the process being analyzed. Different categories of wavelet and various types of wavelets within each category provide a multitude of options to choose from when analyzing a process of interest [*Foufoula-Georgiou and Kumar*, 1994].

[23] The complex Morlet function is expressed by equation (3) in its simplest form (where k_0 is the central frequency, which is generally assumed to be 5 or larger to satisfy the wavelet admissibility condition). The Ricker function, which is a real function, is mathematically represented by equation (4).

$$\psi_M(t) = \frac{1}{\pi^{1/4}} \cdot e^{i2\pi k_0 t} e^{-t^2/2} \tag{3}$$

$$\psi_R(t) = (1 - t^2) \cdot e^{-t^2/2} \tag{4}$$

[24] According to the uncertainty in the Heisenberg principle, there is a lower limit to the product of frequency and time resolution. Thus, as time resolution is improved, frequency resolution degrades and vice versa [*Addisson*, 2004].

[25] The Morlet function provides a lower area of the Heisenberg cell than the derivatives of the Gaussian wavelet functions and retrieves accurate wavelengths at higher signal-to-noise ratios and lower sample frequencies. The wavelet analysis of the synthetic signals confirms this. The Morlet wavelet function (Figure 6) retrieves frequencies of the order of ripples for sampling frequencies below 0.25 m, and the efficiency of the derivatives of the Gaussian wavelet function improves as the order of the derivative is increased. This efficiency of the Morlet wavelet function is particularly important to retrieve frequencies of the order of ripples, and therefore is used for all the estimations with wavelet transforms. These estimations are performed by using a modified version of the wavelet software provided by *Torrence and Compo* [1998].

2.3.2. Discrimination Method

[26] For each synthetic signal and Río Paraná BFP, the separation procedure encompasses the following steps and is valid for either h or η signals:

[27] 1. The continuous wavelet analysis is performed on the original signal (e.g., h in Figure 7 and η in Figure 8). The global wavelet spectrum (Figures 7c and 8c) provides

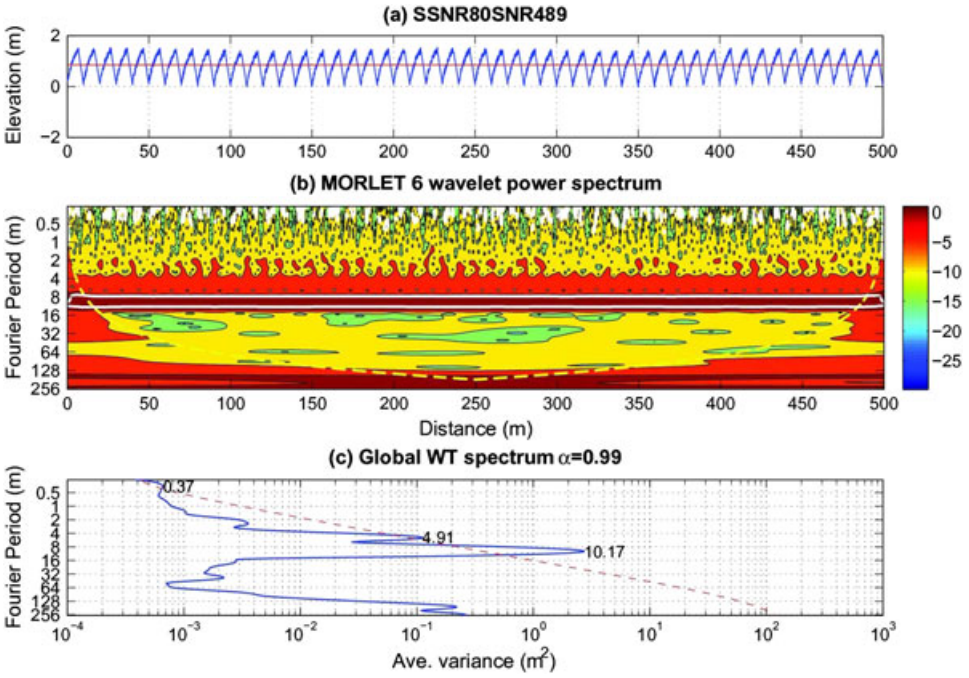

Figure 8. Wavelet analysis output for synthetic signal SSNR80SNR489 (refer to Figure 7 for details concerning the definition of the graphical representations). Note the limitation of the wavelet transforms to retrieve wavelengths that are located closer to the edge of the cone of influence.

information to find the wavelength of the bar scale wave (e.g., 192 m for the synthetic signal named SSNR80SNR489, and 337 m for the BFP named $j = 100$ from the Río Paraná). For the same instances, the global wavelet spectrum also indicates that the dunes have wavelengths of the order of ~ 10 and ~ 62 m, respectively.

[28] 2. The original signal (e.g., η in Figure 10 or h in Figure 9) is filtered by using the robust spline filter with several values of the parameter s. A wavelet transform analysis is then performed for each filtered signal and the one that has a mean wavelength ~ 337 m for $j = 100$ (or ~ 192 m for SSNR80SNR489) is found. This signal becomes the third

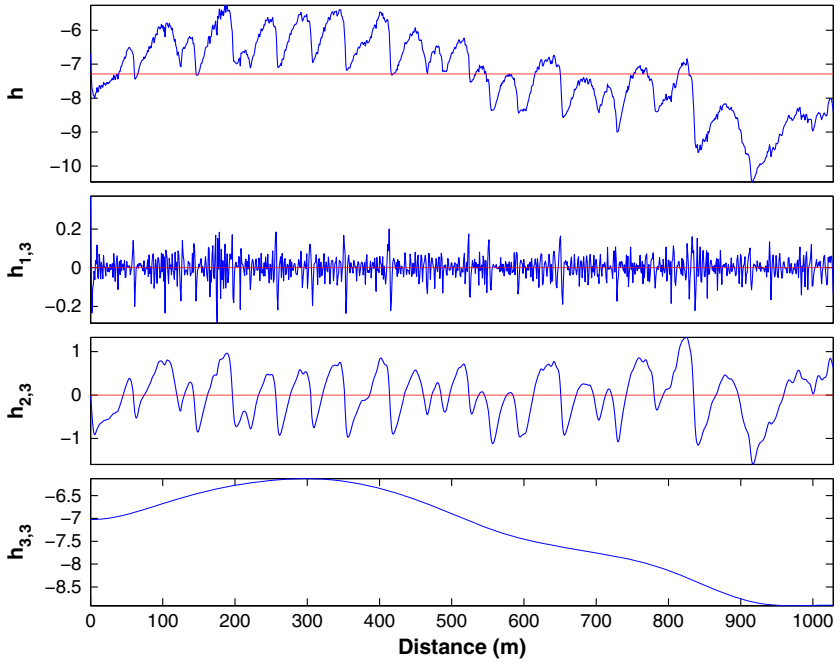

Figure 9. Wavelet-spline discrimination output for section $j = 100$. $h_{1,3}$ represents the first bed form hierarchy (small dunes), $h_{2,3}$ represents the second bed form hierarchy (large to medium size dunes), and $h_{3,3}$ represents the third bed form hierarchy (bars).

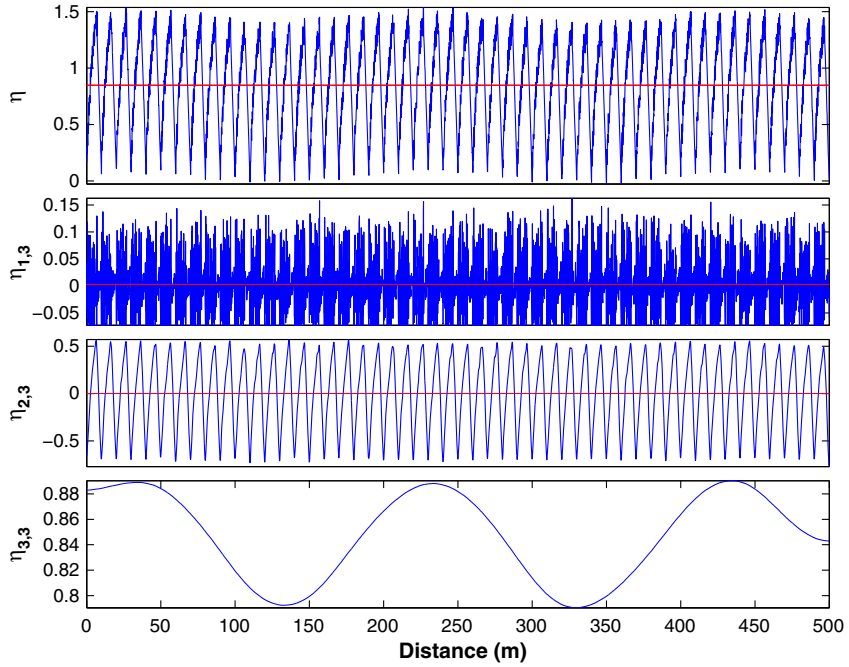

Figure 10. Wavelet-spline discrimination output for the synthetic signal SSNR80SNR489. $\eta_{1,3}$ represents the first bed form hierarchy (ripples), $\eta_{2,3}$ represents the second bed form hierarchy (dunes), and $\eta_{3,3}$ represents the third bed form hierarchy (bars).

level of bed form discrimination ($h_{3,3}$ in Figure 9 and $\eta_{3,3}$ in Figure 10).

[29] 3. $\hat{h}_3$ (or $\hat{\eta}_3$ for the synthetic signals) is defined as $\hat{h}_3 = h - h_{3,3}$ and contains the signal of dunes with superimposed smaller dunes (or superimposed ripples for the synthetic signals).

[30] 4. The $\hat{h}_3$ signal (or $\hat{\eta}_3$ for the synthetic signals) is filtered by using the robust spline filter with different values of the parameter s, to obtain several dune-like signals, named $\hat{h}_2(s)$. For the case of synthetic signals, several ripple-like signals, named $\hat{\eta}_2(s)$, are obtained.

[31] 5. The $\hat{h}_3$ signal is subtracted from each $\hat{h}_2(s)$ to obtain a set of smaller dune-like signals, named $\hat{h}_1(s)$ (or ripple-like signals, named $\hat{\eta}_1(s)$ for the synthetic signals).

[32] A wavelet analysis is performed on each $\hat{h}_1(s)$ and thus the wave with a mean wavelength of 5 m (an arbitrary threshold that defines small dunes for $j = 100$) is obtained. For the case of the synthetic signal, the wave with a mean

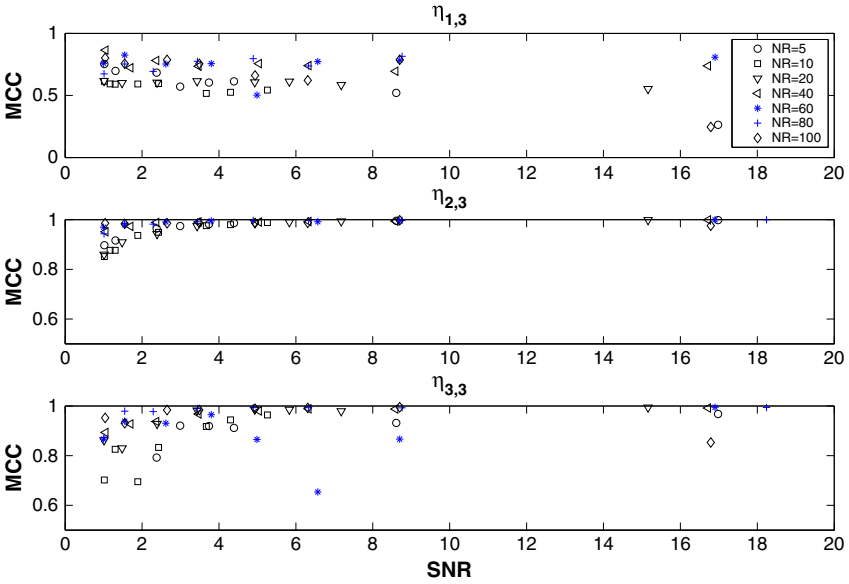

Figure 11. Maximum cross correlation (MCC) between retrieved and actual (a) ripple, (b) dune, and (c) bar synthetic signals.

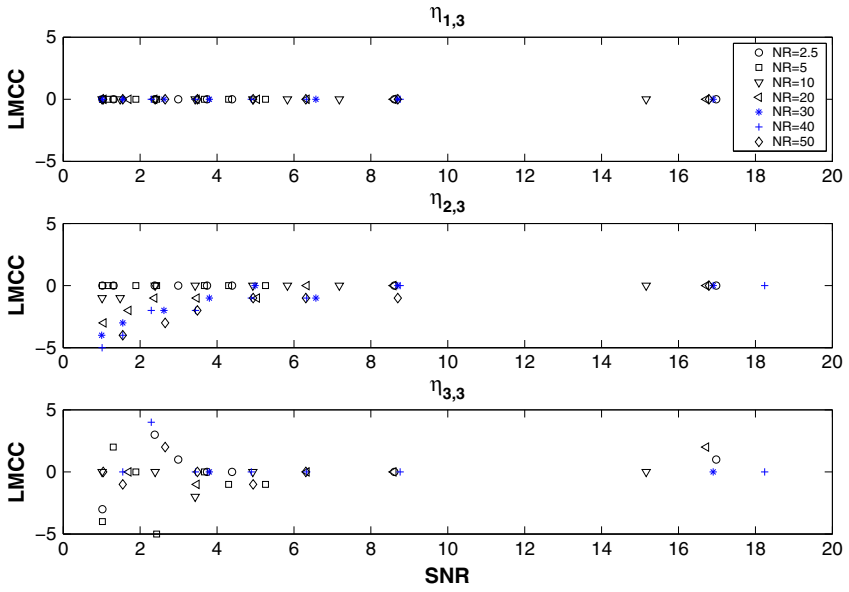

Figure 12. Lag at the maximum cross correlation (LMCC) between retrieved and actual (a) ripple, (b) dune, and (c) bar synthetic signals.

wavelength of 0.6 m (an arbitrary threshold that defines ripples) is obtained. These criteria are, as stated above, one currently accepted criteria used to define ripples and small dunes. The resultant signals obtained then become the first level of the bed form discrimination ($\eta_{1,3}$ in Figure 10 and $h_{1,3}$ in Figure 9), and the corresponding $\hat{\eta}_2(s)$ and $\hat{h}_2(s)$ becomes the second level of bed form separation ($\eta_{2,3}$ in Figure 10 and $h_{2,3}$ in Figure 9).

[33] It is important to point out that the steps outlined above are performed on preprocessed data where no outliers are present, as was the case of the bed form data obtained by *Parsons et al.* [2005].

3. Results

3.1. Accuracy of the Method

[34] The accuracy of the method is assessed by analyzing the synthetic signals. Our results reveal that the method provides a high accuracy in retrieving information from the bar and dune form scale signals. A cross-correlation analysis of the retrieved and actual bar and dune signals is persistently higher than 0.9 at lags equal to zero for NR > 25 at any SNR (see Figures 11b–11c and Figures 12b–12c). Likewise, their standard deviation ratios (Figures 13b and 13c) are markedly closer to a value of unity for NR > 25 at any SNR.

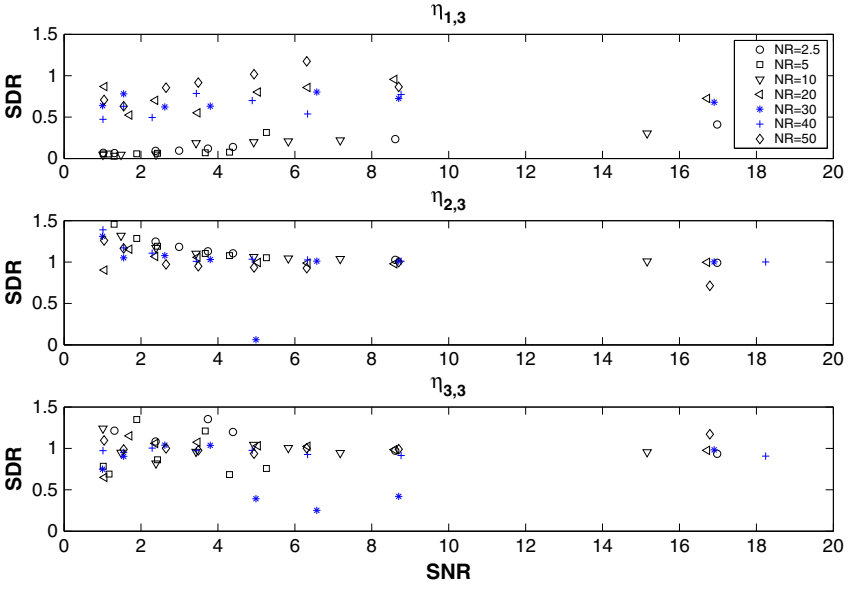

Figure 13. Standard deviation ratio (SDR) between retrieved and actual (a) ripple, (b) dune, and (c) bar synthetic signals.

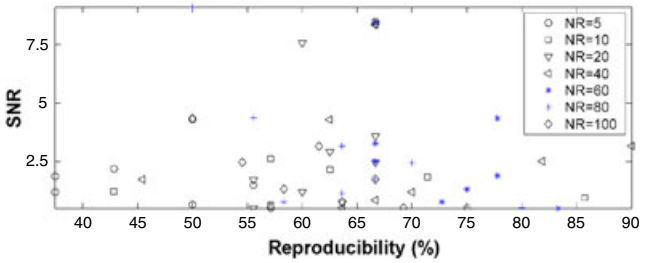

Figure 14. Reproducibility of the synthetic ripple frequencies.

Filters necessarily induce some deformation to the signals [*Raja et al.*, 2002; *Mostacci et al.*, 2010], and this is critical for retrieving higher-frequency ripple signals. A closer analysis of these signals indicates that the cross correlation between the actual and recovered signals is higher than 75% for NR > 25 (see Figure 11a), and that the robust spline filter does not lag the ripple signal, as shown in Figure 12a. However, the robust spline filter does distort the amplitudes (see Figure 13a), especially for NR > 25 and SNR < 5, with most of the amplitude deformations occurring in the bed form troughs. It is important to note that among the different filters, the robust spline filter minimizes such trough deformation [*Raja et al.*, 2002]. Our results reveal that this limitation of the filters is improved when the points of the ripple signal with negative elevations, and below 2.5 times the standard deviation threshold, are considered as outliers, and are therefore fixed at such a threshold.

[35] In order to assess the reproducibility of the ripple frequencies, the reproducibility ratio, defined as the ratio between the number of common peaks (of the actual and retrieved ripple signals) detected in at least 50% of the whole spectra and the total number of peaks corresponding to the number of peaks detected across all the spectra [*Mostacci et al.*, 2010], was quantified. These results highlight that the reproducibility is higher than 70% for NR > 25 (Figure 14).

[36] The methodology also shows good performance when applied to the synthetic data that exhibits a higher variability. The analysis again reveals a higher efficiency in retrieving bars and dunes than for the case of ripples. Figure 16 presents an instance of the synthetic signal and

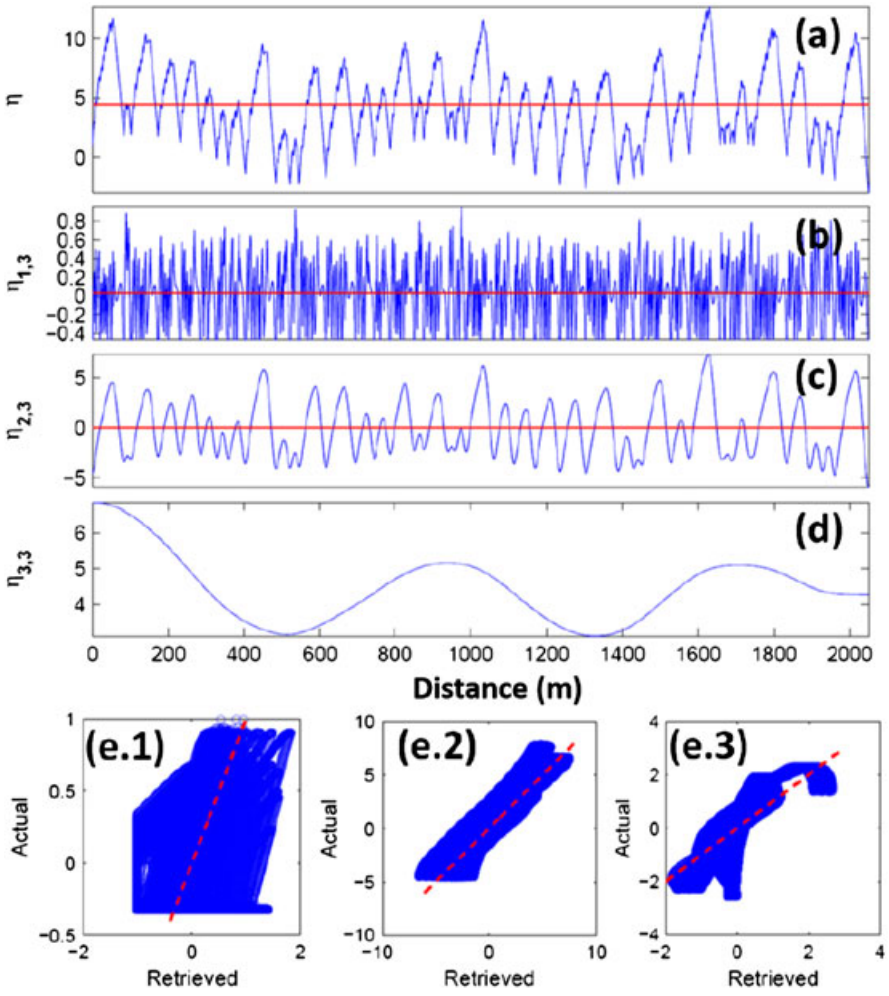

Figure 15. Discrimination of synthetic signals exhibiting a higher variability. (a) Synthetic signal comprised of ripples, small dunes, medium dunes, and bars; (b) retrieved ripple signal, (c) retrieved dune signal; (d) retrieved bars signal; (e.1) retrieved ripples, (e.2) retrieved dunes; and (e.3) retrieved bars. In all cases, the red dotted line represents a line with unitary slope.

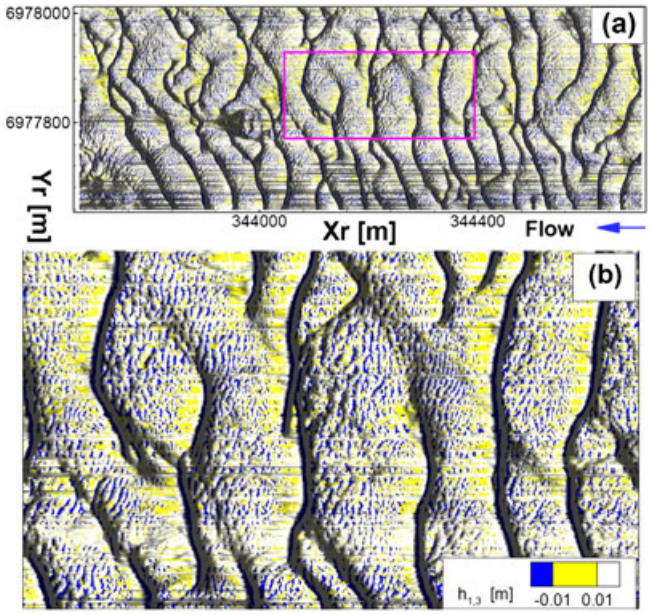

Figure 16. (a) $h_{1,3}$ (small dunes) data of the Río Paraná survey and (b) inset of small dunes superimposed on markedly three-dimensional larger dunes. Here the smaller dunes (yellow areas) concentrate in the trough region of the larger dunes and grow in amplitude as they get closer to the crests of the larger bed forms. Flow is from right to left. X_r represents the relative Easting and Y_r the relative Northing.

a set of results from the analysis, and shows that the best results are achieved for NR > 30.

3.2. Discrimination of Bed Form Scales at the Field Site

[37] After the procedure outlined above is applied to the 370 field site BFPs, various scales of bed forms are found (Figures 15, 17, 18). Figure 15b shows that for the case of markedly 3-D medium and large dunes, the small dunes with higher amplitudes are concentrated near to the larger dune troughs and their amplitudes tend to increase as they near the crests of the larger dunes, denoting that the process of bed form amalgamation is prevalent for 3-D dunes. This pattern is absent for large dunes that are more 2-D and with crests subparallel with their neighbors, and may be explained by the fact that obliquity of the crestline influences the length of any flow separation zone and thus influences the magnitudes of the leeside Reynolds stresses, drag coefficients, and the dispersal patterns of sediments [*Best*, 2005]. Indeed, Figure 17 shows that crestal platforms are commonly present over 3-D large dunes. According to *Maddux et al.* [2003] and *Venditti* [2007], turbulence generated by 3-D dunes is weaker than that in the 2-D case, due to the generation of secondary flows over the 3-D forms, perhaps highlighting a process of the crest having conditions transitional to an upper stage plane bed. Figure 18 shows that the bar is highly variable along the survey area, and thus a linear representation of this feature is too simplistic.

[38] A wavelet analysis using the Morlet wavelet function (equation (3)) on the $\hat{h}_3$ signals was also conducted, and the average wavelet power spectrum, namely the power Hovmöller, for 4–8 m and 8–16 m bands was obtained. The power Hovmöller is a 2-D contour plot used to display the wavelet variance of the bed form profile along the x axis at distinct transverse locations, y. This 2-D contour plot allows assessment of the variability of the power distribution in both the longitudinal and transverse directions, as well as isolation of features characterized by a certain range of dimensions, such as wavelength [*Catano-Lopera et al.*, 2009]. Figure 19a indicates that the higher-frequency bed forms are located mainly in the troughs and in the lower portions of the stoss sides of the larger dune forms. Likewise, Figure 19b indicates that the second band is densely distributed with large dunes, especially close to the troughs.

[39] Since the methodology analyses stream-wise transects, it has the potential to locate the crests and troughs of the bed form hierarchies present in the study area even for temporally repeated bed form analyses, although it is limited in fully describing the three-dimensional nature of the bed forms.

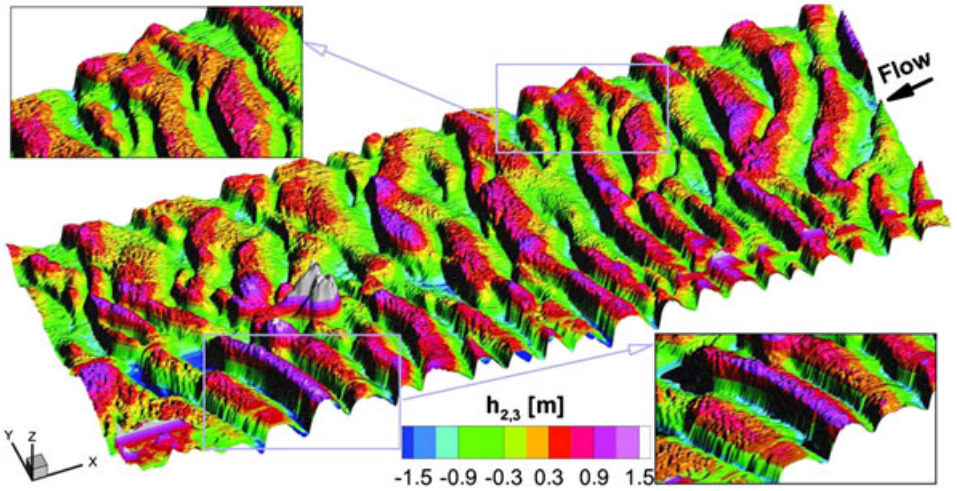

Figure 17. $h_{2,3}$ (medium to large dunes) data of the Río Paraná survey. Note that crestal platforms are developed on the shallower, markedly three-dimensional, larger dunes. Subparallel larger dunes tend to be more two-dimensional. Bed forms migration is from right to left.

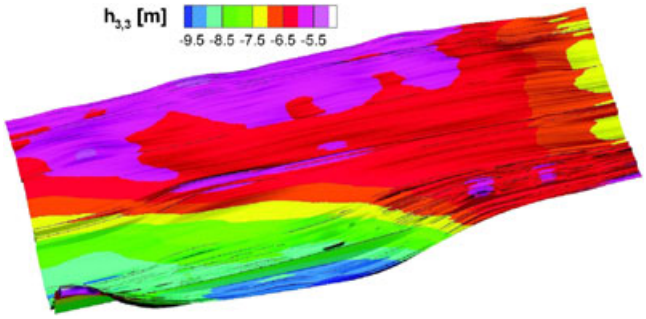

Figure 18. $h_{3,3}$ (bars) data of the Río Paraná survey. Flow is from right to left. This bed form hierarchy imposes a highly nonstationary condition on the BFPs. A linear representation of this feature would be too simplistic for this survey.

3.3. The Statistics of Bed Form Features

[40] The data for different sized bed forms, filtered as the signal of the smallest bed forms over the stoss side of the larger dunes, are analyzed statistically later. The histograms of the dune descriptors (see Figure 20a–20f) show that there is a marked difference in the distribution of the wavelength of smaller features on the lee and stoss sides. Similar results have been reported by *Jackson* [1976], *Gabel* [1993], *Kheiashy et al.* [2007], and *Knaapen* [2008]. Our results also indicate that there is a strong correlation between the wavelength and amplitude of the superimposed smaller dunes on the stoss side; conversely, the same parameters are not correlated on the lee side.

[41] The probability distribution functions (PDFs) of the dimensionless descriptors of the large and small dunes, together with the Weibull, Gaussian, Gamma, GEV, and Pareto distributions, are shown in Figure 21. In each case, the dimensionless value of each descriptor is defined as the descriptor divided by its mean value. The goodness of fit of some distribution functions was also evaluated by the normalized Anderson-Darling test (normalized with the Gamma A2, denoted A2*, see Table 1), that allows testing of a wider range of distributions when some of the parameters may not be known [*Dodge*, 2008]. The minimum A2* value denotes the best fit to the PDF. In most of the cases (Figures 21a–21d and Table 1), the Gamma distribution provides the best goodness of fit. Likewise, all the parameters show a positive skewness and leptokurtic distribution.

[42] A similar analysis was performed on the small dune sample population (Figures 22a and 22b; Table 1). The histograms (Figure 20d–20f) demonstrate that the wavelength of these bed forms on both the stoss and lee sides present the characteristics of discrete variables. On the other hand, the absolute value of their amplitudes reveals that the characteristic amplitude is approximately 0.05 m. These slopes, when compared to that of the dunes, present lower values for the stoss side but similar values in the lee side. The Gamma distribution presents the best goodness of fit, with the kurtosis being positive and greater than that of the larger dunes, and possessing a leptokurtic distribution. The recurrence of the Gamma PDF as the best descriptor of the probability density function justifies normalizing the Anderson-Darling test results with the Gamma's A2.

4. Discussion

4.1. Discrimination Method

[43] The new methodology proposed herein is based on the scaling definition of dunes and ripples, is applicable to laboratory and field measurements and overcomes the limitations of using a moving average and spectral analysis. The methodology also allows the user to define a third level based on the potential scales of interest.

[44] The present methodology has successfully discriminated larger bars and different scales of dunes. By analyzing synthetic signals, the procedure has also been shown to perform well in retrieving and quantifying the various scales of signal within a bed form series (up to the third-level wave) when at least one period of such a wave is present in the BFP, although it does impose some waviness where no single period is present. Therefore, there is an uncertainty in the present results, although this is imposed by the data length rather than the methodology. Since the methodology solves for the "*s*" parameter that minimizes this limitation, the retrieved larger-scale signal is still more suitable than using a linear trend line [e.g., *van der Mark and Blom*, 2007] that may not be applicable for large rivers such as the Río Paraná, where the mean river bed level fluctuates over long distances.

[45] Some researchers [*van der Mark and Blom*, 2007; *Gabel*, 1993] highlight that the definition of ripples as bed forms that have wavelengths less than 0.60 m is restrictive, although other researchers [e.g., *Leclair*, 2002] have successfully used such a threshold. *Coleman and Nikora* [2011] suggest the use of a threshold bed form height to distinguish transient sand pileups from stable bed forms that offer a resistance to flow. The estimates presented herein demonstrate that, even though the ripple definition is limited, when coupled with the capabilities of both robust spline filters and wavelet transforms, such widely used discrimination criteria

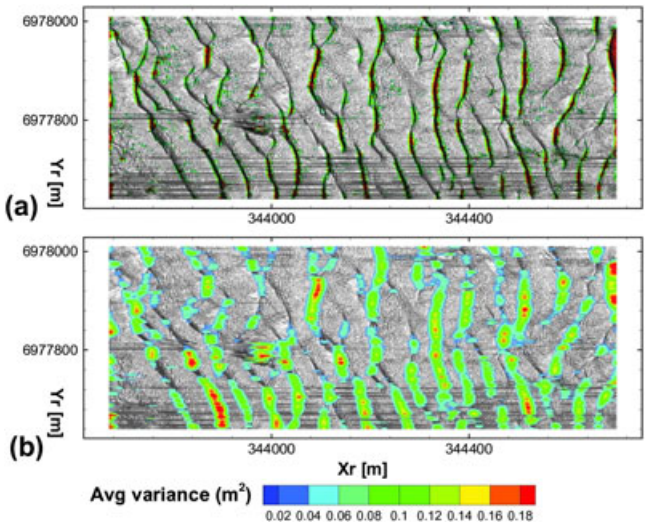

Figure 19. Power Hovmöller of the averaged wavelet power spectrum for two scale bands of the $h_{2,3}$ swath: (a) [4–8] m (small dunes), (b) [8–16] m (medium size dunes). In all cases, the contours present the variance with a 95% confidence level. X_r represents the relative Easting and Y_r the relative Northing.

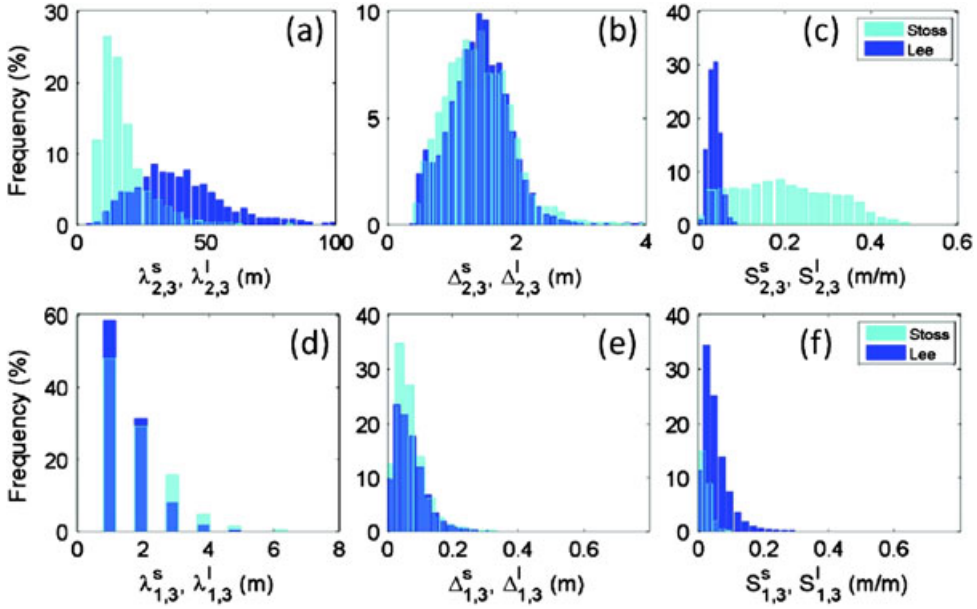

Figure 20. Histograms of the large dune descriptors: (a) The wavelength of the lee side $\left(\lambda^l_{2,3}\right)$ shows higher variability than that of the stoss side; (b) the amplitudes of the stoss and lee sides ($\Delta^s_{2,3}$ and $\Delta^l_{2,3}$), respectively, show a similar distribution of frequencies; (c) the slope of the stoss side $\left(S^s_{2,3}\right)$ shows an almost symmetrical distribution; however, the slope of the lee side $\left(S^l_{2,3}\right)$, that is closely related to the angle of repose of the sediment, shows higher variability. Histograms of the small dune descriptors: (d) the wavelengths of the stoss and lee sides ($\lambda^s_{2,3}$ and $\lambda^l_{2,3}$), respectively, in the continuity of the interval are strongly determined by the sampling frequency; (e) the amplitudes of the stoss and lee sides ($\Delta^s_{2,3}$ and $\Delta^l_{2,3}$), respectively, show a similar distribution. The small dunes, which represent shorter life-span structures, do not appear to be related to the angle of repose of the sediment; (f) plot illustrating there is no marked variability between the lee and stoss slopes.

can retrieve relevant information for ripples and dunes for both their lee and stoss sides. Unfortunately, few studies have focused on the transitional areas between bed form states [e.g., see *Best*, 1996; *Best and Robert*, 2006], even though they are critical to explain bed form scales.

[46] The method proposed herein shows potential in retrieving the ripple signal with a reasonable level of accuracy, as demonstrated by the results of the synthetic signals analysis. Moreover, by using wavelet transforms, the distribution of the wavelengths of small dunes can also be estimated, and by using the robust spline filter, the distribution of the amplitude of bed forms within the Río Paraná can be quantified and robustly assessed.

4.2. The Statistics of Bed Forms

[47] The bed morphology of the Río Paraná comprises bars (unit, point, complex bars), dunes (of various scales) and ripples with a three-dimensional morphology [*Parsons et al.*, 2005]. Bars have wavelengths from 325 to >450 m, and generally larger bars are associated with larger dunes. A similar trend has also been reported by *Komarova and Newell* [2000], who studied the possible interaction between dunes and bars and showed that the nonlinear coupling between relatively short (dunes) and long (bars) wavelength bed forms may cause the growth of bars.

[48] In many instances in the present analysis, the dune signals show that higher trough-scour depths relative to mean bed level are proceeded by a higher upstream dune. Indeed, the dunes within the present reach are markedly asymmetric, with the lee slope being nearly four times that of the stoss slope. As shown in Figure 4, the small dunes exhibit irregular three-dimensional features, which are similar to linguoid ripples that form under higher bed shear stresses or have had longer development times and represent the second stage of the transition from ripples to dunes [*Robert and Uhlman*, 2001].

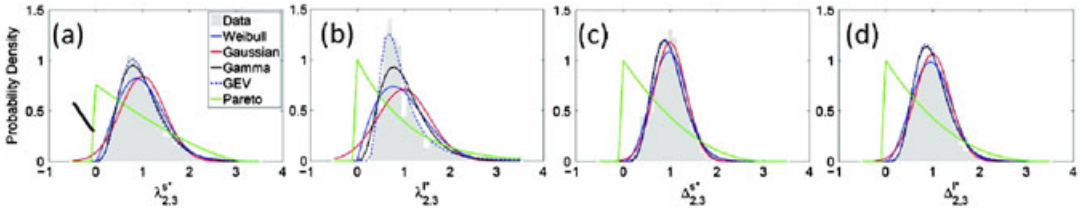

Figure 21. Probability distribution of the larger dunes dimensionless descriptors: (a) stoss amplitude, (b) lee amplitude, (c) stoss wavelength, and (d) lee wavelength.

Table 1. Normalized Anderson-Darling Test Results[a]

Descriptor	Gaussian	Weibull	Gamma	LEV
$\Delta^{l^*}_{1,3}$	50.9	5.9	1.0	5.2
$\lambda^{l^*}_{1,3}$	1.0	0.9	1.0	1.1
$S^{l^*}_{1,3}$	9.4	1.4	1.0	3.2
$\Delta^{s^*}_{1,3}$	45.7	3.4	1.0	6.1
$\lambda^{s^*}_{1,3}$	0.9	0.9	1.0	1.2
$S^{s^*}_{1,3}$	29.0	3.0	1.0	5.4
$\Delta^{l^*}_{2,3}$	2.5	3.0	1.0	2.3
$\lambda^{l^*}_{2,3}$	3.4	2.2	1.0	0.7
$S^{l^*}_{2,3}$	0.5	0.5	1.0	0.6
$\Delta^{s^*}_{2,3}$	0.2	0.7	1.0	1.7
$\lambda^{s^*}_{2,3}$	13.3	6.5	1.0	0.6
$S^{s^*}_{2,3}$	8.0	14.1	1.0	2.5

[a]The minimum value defines the standard probability density function that best describes a given normalized bed form geometric descriptor

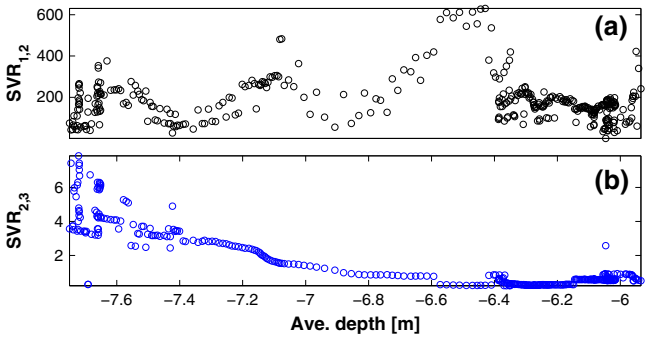

Figure 23. (a) $SVR_{1,2}$ (scale-variance-ratio between small and medium-large dunes), indicating no correlation with the averaged water depth, a characteristic similar to that of ripples. Conversely, (b) $SVR_{2,3}$ (scale-variance-ratio between medium-large dunes and bars), shows a strong dependence on the average water depth, as a characteristic of the dunes.

[49] If, similar to the signal-to-noise ratio, the scale-variance-ratio ($SVR_{i,j}$) is set as the ratio between the standard deviation of the hierarchy i and that of the hierarchy j (for $i < j$), the present results show that $SVR_{1,2}$ (SVR between small dunes and medium-large dunes) is not correlated to the average water depth (see Figure 23a); the cross correlation between these signals is –3%. This implies that, similar to ripples, the height of the small dunes is not highly dependent on the water depth. This finding may be explained by some of the descriptors of the small dunes being governed by the local boundary layer thickness and thus being independent of the water depth [*Engelund and Fredsøe*, 1982]. On the contrary, $SVR_{2,3}$, the SVR between the medium-large dunes and bars (see Figure 23b), shows high dependence on the average water depth (the cross correlation between these signals is –87%), a relationship also noted in past work [*Richards*, 1980; *Raudkivi*, 1997; *Coleman and Eling*, 2000; *Charru and Hinch*, 2006; *Colombini and Stocchino*, 2011; *Coleman and Nikora*, 2011]. Therefore, $SVR_{i,j}$ has the potential to become a robust frame in which to verify the accuracy of discrimination.

[50] In the present study, the Anderson-Darling test was used to estimate the goodness of fit of the PDFs, which in past work has been assessed using a relative error [*van der Mark et al.*, 2008a] and the Kolmogorov-Smirnov test [*van der Mark et al.*, 2008b]. However, the Kolmogorov-Smirnov test presents two main limitations: (1) it tends to be more sensitive near the center of the distribution than at its tails, and (2) perhaps a more serious limitation is that the distribution must be fully specified. Importantly, if the location, scale, and shape parameters are estimated from the data, then the critical region of the Kolmogorov-Smirnov test is no longer valid and typically must be determined by simulation [*NIST/SEMATECH*, 2010]. Use of the Anderson-Darling test, as proposed herein, overcomes these limitations and appears a more useful technique.

[51] The PDFs of the dimensionless descriptors of bed form characteristics vary for different hierarchies. The PDFs that best describe the dune descriptors are the Gamma and Weibull functions, whereas the smaller dunes are best represented by the Gamma distribution. In all cases, the PDFs possess a positive skewness and leptokurtic distributions. Past studies [*Annambhotla et al.*, 1972; *van der Mark et al.*, 2008a] did not analyze the PDFs of the stoss and lee descriptors and highlighted that the PDFs are very sensitive to the preprocessing procedure. However, it is important to note that some of these studies found that both dune and ripple elevations are best described by the Gamma PDF [*Paola and Borgman*, 1991; *Leclair et al.*, 1997], whereas others found that the wavelengths, amplitudes, and heights are best described by an exponential probability law [*Annambhotla et al.*, 1972].

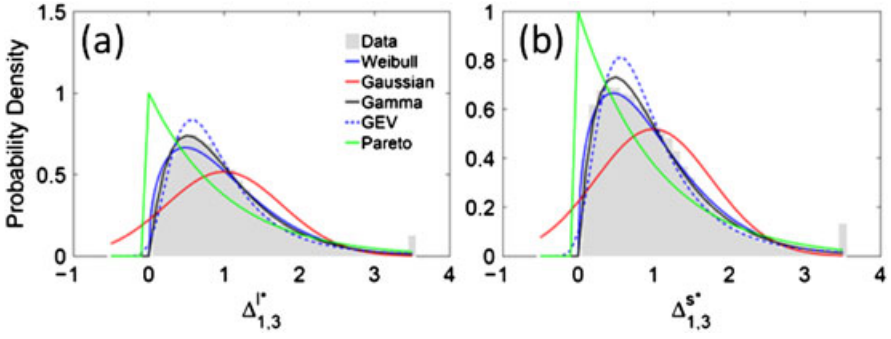

Figure 22. Probability distribution of the small dunes dimensionless descriptors: (a) lee amplitude, (b) stoss amplitude.

5. Conclusions

[52] The discrimination of different scales of bed forms is important in order to study the geometric variability and quantify the influence of bed forms on the flow field and flow resistance. The present paper has developed a methodology that combines the capabilities of continuous wavelet transforms and a robust spline filter to discriminate waves with different periodicities in bed form profiles, and has applied this methodology to 3-D bed form data from the Río Paraná, Argentina.

[53] This method uses a symbolic representation of bed form descriptors (e.g., wavelength, amplitude, slope) for each hierarchy (e.g., small dunes, dunes, bars) and determines a delimitation of such descriptors that is in-line with past model, laboratory, and field studies. The procedure has successfully retrieved the descriptors of the dunes scales for both the bed form stoss and lee sides.

[54] The synthetic bed forms considered herein comprise wavelength scales with ranges up to four orders of magnitude (e.g., bars of 200 m down to ripples of 0.1 m). For such a spectrum, the methodology proposed herein effectively retrieved information concerning the bars and dunes with a high accuracy for NR > 25 and SNR closer to 5. For the case of ripples, the method retrieves a signal that is 75% correlated with the actual signal for NR > 25. Likewise, the method retrieves around 70% of the wavelengths and 70% of the actual ripple amplitudes when the NR is higher than 25, but slightly decreases as the NR is increased. In cases where the frequency range is higher, the accuracy will tend to decrease as explained by the Heisenberg uncertainty principle. The analysis performed on synthetic data exhibiting higher variability also reveals that the method is efficient for NR > 30. Likewise, this methodology has shown to be robust when applied to bed form discrimination in the Río Paraná, Argentina and allows separation of bar and various scales of dunes, which are superimposed on each other and on the larger bar forms.

[55] One-dimensional wavelet transforms are not able to differentiate between a two-dimensional and a three-dimensional bed form feature. Since bed forms in natural channels are predominantly three-dimensional in planform, their scale discrimination could be greatly assisted by the application of two-dimensional wavelet transforms and coupled with two-dimensional robust spline filters as proposed herein.

Notation

- x Relative distance.
- Δx Sampling interval.
- Δx_N Nyquist sampling interval.
- X_r, Y_r Relative Easting and Northing obtained by rotating a bed form parcel toward the East-West orientation.
- SNR Signal-to-noise ratio.
- NR Nyquist rate.
- BFP Bed form profile.
- f'' Form resistance.
- s A real positive scalar that controls the degree of smoothing of the robust spline filter.
- k Normalized length of the stoss face.
- S_b Slope to the synthetic bar.
- $\psi_M(t)$ Morlet wavelet function.
- k_0 Central frequency of the Morlet wavelet function.
- $\psi_R(t)$ Ricker wavelet function (also known as Mexican hat wavelet function).
- h Water depth; It is also used to represent mean water depth in *Yalin and Lai* [1985].
- $\langle d \rangle$ Mean water depth.
- $h_{i,j}$ Water depth of the bed form hierarchy i when j bed form hierarchies are considered in the analysis.
- $\hat{h}_i(s)$ Smoothed version of the water depth for a given "s" parameter of the robust spline filter.
- η Bed form elevation.
- $\hat{\eta}_i(s)$ Smoothed version of the bed form elevation for a given "s" parameter of the robust spline filter.
- η_b Distance from the mean elevation to a downstream trough.
- η_c Distance from the crest to the mean elevation.
- η_t Distance from the mean elevation to a trough.
- $\eta_{i,j}$ Bed form elevation of the bed form hierarchy i when j bed form hierarchies are considered in the analysis. For specific representations of the lee and stoss side, the superscripts l and s are used.
- ϕ Phase of the synthetic bar sinusoidal function.
- Λ Dune wavelength in *Yalin and Lai* [1985].
- λ General symbolic expression for the wavelength; it is also used to represent ripple wavelength in *Yalin and Lai* [1985].
- $\lambda_{i,j}$ Wavelength of the bed form hierarchy i when j bed form hierarchies are considered in the analysis.
- λ_c Wavelength defined as the linear distance between two consecutive crests.
- λ_l Either linear or aligned distance between a crest and the downstream trough.
- λ_s Either linear or the aligned distance between a crest and the upstream trough.
- $\lambda_{s'}$ Horizontal distance between two points located in the stoss side that exhibit a strong linear trend.
- λ_t Wavelength defined as either the linear or the aligned distance between two consecutive troughs.
- λ_u Wavelength defined as the distance between two consecutive zero upcrossings.
- $\lambda^l_{i,j}$ Wavelength of the lee side at bed form hierarchy i when j bed form hierarchies are considered in the analysis.
- $\lambda^s_{i,j}$ Wavelength of the stoss side at bed form hierarchy i when j bed form hierarchies are considered in the analysis.
- δ Ripple amplitude in *Yalin and Lai* [1985].
- Δ General symbolic expression for amplitude; it is also used to represent dune amplitude in *Yalin and Lai* [1985].
- Δ_l Either linear or the aligned distance between a crest and the downstream trough.
- Δ_s Either linear or the aligned distance between a crest and the upstream trough.
- $\Delta_{s'}$ Vertical distance between two points located in the stoss side that exhibit a strong linear trend.

$\Delta^l_{i,j}$ Amplitude of the lee side at bed form hierarchy i when j bed form hierarchies are considered in the analysis.

$\Delta^s_{i,j}$ Amplitude of the stoss side at bed form hierarchy i when j bed form hierarchies are considered in the analysis.

$\Delta_{i,j}$ Amplitude of the bed form hierarchy i when j bed form hierarchies are considered in the analysis.

$S^l_{i,j}$ Steepness of the lee side at bed form hierarchy i when j bed form hierarchies are considered in the analysis.

$S^s_{i,j}$ Steepness of the stoss side at bed form hierarchy i when j bed form hierarchies are considered in the analysis.

MCC Maximum cross correlation between the retrieved and actual signal.

LMCC Lag at the maximum cross correlation between the retrieved and actual signal.

SDR Standard deviation ratio between the retrieved and actual signal.

PDF Probability density function.

$A2^*$ Normalized (with the Gamma's A2) Anderson-Darling test parameter. The minimum $A2^*$ value denotes the best fit to a given PDF.

$\mathrm{SVR}_{i,j}$ Ratio between the standard deviation of the bed form hierarchy i and that of the bed form hierarchy j ($i < j$).

$\Xi = \frac{\Delta^2}{\Lambda h}$ Proxy parameter to quantify the form resistance in *Yalin and Lai* [1985].

Note: The normalized versions of the bed form descriptors $\lambda^{l*}_{i,j}$, $\lambda^{s*}_{i,j}$, $\Delta^{l*}_{i,j}$, and $\Delta^{s*}_{i,j}$ are obtained by dividing the descriptor by its mean.

[56] **Acknowledgments.** We thank Yovanni Catano, Michael Lamb, and Anthony Dalrymple for technical discussion on topics related to bed forms and signal analysis. This study was conducted thanks to J.D. Abad's startup funding from the Department of Civil and Environmental Engineering, University of Pittsburgh. Thanks to Dr. Orfeo for sharing the bathymetric data of the Paraná River. We also thank the Peruvian Navy staff, particularly to Commander Hugo Montoro for technical discussion on the practical applications of the method.

References

Abad, J. D. (2009), Planform dynamics of meandering channelss based on wavelet analysis, Abstract H41B-0891 presented at 2009 Fall Meeting, AGU, San Francisco, Calif.

Aberle, J., V. Nikora, M. Henning, B. Ettmer, and B. Hentschel (2010), Statistical characterization of bed roughness due to bed forms: A field study in the Elbe River at Aken, Germany, *Water Resour. Res.*, *46*, W03521, doi:10.1029/2008WR007406.

Addisson, P. (2004), *The Illustrated Wavelet Transform Handbook*, 420 p., Institute of Physics Publishing Bristol and Philadelphia, United Kingdom.

Allen, J. R. L. (1982), *Sedimentary Structures: Their Character and Physical Basis*, 663 p., vol. Volume I, Elsevier Scientific Publishing Company, The Netherlands.

Amsler, M. L., and M. H. Garcia (1997), Discussion: Sand-dune geometry of large rivers during floods, *J. Hydraul. Eng.*, *123*, 582–585.

Annambhotla, V. S. S., W. W. Sayre, and R. H. Livesey (1972), Statistical properties of Missouri River bed forms, *J. Waterway. Div.*, *98*(4), 489–510.

Ashley, G. M. (1990), Classification of large-scale subaqueous bedforms: A new look at an old problem, *J. Sediment. Petrol.*, *60*(1), 160–172.

Baas, J. A. (1999), An empirical model for the development and equilibrium morphology of current ripples in fine sand, *Sedimentology*, *46*, 123–138.

Baulinas, S. (1997), Time scales and trends in the central England temperature data (1659 1990): A wavelet analysis, *Geophys. Res. Lett.*, *24*, 1351–1354, doi:10.1029/97GL01184.

Bennett, S. J., and J. L. Best (1996), Mean flow and turbulence structure over fixed ripples and the ripple-dune transition, in *Coherent Flow Structures in Open Channels*, edited by P. J. Ashworth et al., pp. 281–304, John Wiley, Chichester.

Best, J. (2005), The fluid dynamics of river dunes: A review and some future research directions, *J. Geophys. Res.*, *110*, F04S02, doi:10.1029/2004JF000218.

Best, J., and A. Robert (2006), Discussion of "Transition from Ripples to Dunes" by A.J. Raudkivi, *J. Hydraul. Eng.*, *132*(12), 1316–1320.

Best, J. L. (1996), The fluid dynamics of small-scale alluvial bedforms, in *The Fluid Dynamics of Small-Scale Alluvial Bedforms*, edited by P. A. Carling, and M. R. Dawson, pp. 67–125, John Wiley and Sons, Chichester.

Blom, A., and M. G. Kleinhans (2007), Estimating bed form height from sorting preserved in sedimentary records of river dunes, deltas and bars, in *5th IAHR Symposium on River, Coastal and Estuarine Morphodynamics*, edited by C. M. Dohmen-Janssen, and S. J. M. H. Hulscher, pp. 641–648, International Association of Hydro-Environment Research, Enschede, NL.

Blom, A., and G. Parker (2004), Vertical sorting and the morphodynamics of bed form-dominated rivers: A modeling framework, *J. Geophys. Res.*, *109*, F02007, doi:10.1029/2006JF000618.

Brinke, W. B. M. T., A. W. E. Wilbers, and C. Wesseling (1999), Dune growth, decay and migration rates during a large-magnitude flood at a sand and mixed sand-gravel bed in the Dutch Rhine river system, in *Fluvial Sedimentology VI,* vol. 28, edited by N. D. Smith, and J. Rogers, pp. 15–32, Blackwell Publishing Ltd., Oxford, UK.

Cardenas, M. B., and J. L. Wilson (2006), The influence of ambient groundwater discharge on exchange zones induced by current bedform interactions, *J. Hydrol.*, *331*, 103–109.

Cardenas, M. B., J. L. Wilson, and V. A. Zlotnik (2004), Impact of heterogeneity, bed forms, and stream curvature on subchannel hyporheic exchange, *Water Resour. Res.*, *40*, W08307, doi:10.1029/2004WR003008.

Cardenas, M. B., J. L. Wilson, and V. A. Zlotnik (2007), Hydrodynamics of coupled flow above and below a sediment-water interface with triangular bedforms, *Adv. Water Resour.*, *30*, 301–313.

Catano-Lopera, Y., J. D. Abad, and M. H. Garcia (2009), Characterization of bedform morphology generated under combined flows and currents using wavelet analysis, *Ocean Eng.*, *36*, 617–632.

Charru, F., and E. J. Hinch (2006), Ripple formation on a particle bed sheared by a viscous liquid. Part 1. Steady flow, *J. Hydraul. Res.*, *550*, 111–121.

Coleman, S. E., and B. Eling (2000), Sand wavelets in laminar open-channel flows, *J. Hydraul. Res.*, *38*(5), 331–338.

Coleman, S. E., and V. I. Nikora (2011), Fluvial dunes: initiation, characterization, flow structure, *Earth Surf. Processes Landforms*, *36*, 39–57.

Colombini, M., and A. Stocchino (2011), Ripple and dune formation in rivers, *J. Fluid Mech.*, *673*, 121–131.

Das, S., N. Mohanty, and A. Singh (2008), Is the Nyquist rate enough?, in *2008 3rd International Conference on Digital Telecommunications (ICDT)*, Institute of Electrical and Electronics Engineers (IEEE), Washington, DC, USA, 27–32.

Dimas, A. A., and G. A. Kolokythas (2011), Flow dynamics and bed resistance of wave propagation over bed ripples, *J. Waterw. Port C. Div.*, *137*(2), 64–74.

Dodge, Y. (2008), *The Concise Encyclopedia of Statistics*, USA, Springer, New York.

Elhakeem, M., and J. Imran (2006), A bedload model for uniform sediment derived from the movement of bedforms, in *River, Coastal and Estuarine Morphodynamics: RCEM 2005*, edited by G. Parker, and M. H. Garcia, pp. 853–860, Taylor and Francis Group, London.

Engelund, F., and J. Fredsøe (1982), Sediment ripples and dunes, *Annu. Rev. Fluid Mechanics*, *14*, 13–37.

Exner, F. (1925), Uber die wechselwirkung zwischen wasser und geschiebe in flüssen, *Akad. Wiss. Wien Math. Naturwiss. Klasse*, *134*(2a), 165–180

Farge, M. (1992), Wavelet transforms and their application to turbulence, *Annu. Rev. Fluid Mech.*, *24*, 395–457.

Felix, M., S. Sturton, and J. Peakall (2005), Combined measurements of velocity and concentration in experimental turbidity currents, *Sediment. Geol.*, *179*, 31–47.

Foufoula-Georgiou, E., and P. Kumar (1994), *Wavelets in Geophysics*, Academic Press, Inc., USA.

Frings, R. M., and M. G. Kleinhans (2008), Complex variations in sediment transport at three large river bifurcations during discharge waves in the river rhine, *Sedimentology*, *55*, 1145–1171.

Gabel, S. (1993), Geometry and kinematics of dunes during steady and unsteady flows in the Calamus River, Nebraska, USA, *Sedimentology*, *40*, 237–269.

Garcia, D. (2010), Robust smoothing of gridded data in one and higher dimensions with missing values, *Comput. Stat. Data Anal.*, *54*(4), 1167–1178.

Ghiene, J.-F., F. Girard, J. Moreau, and J.-L. Rubino (2010), Late Ordovician climbing-dune cross-stratification: A signature of outburst floods in proglacial outwash environments?, *Sedimentology*, *57*, 1175–1198.

Gupta, A. (2007), *Large Rivers: Geomorphology and Management*, 714 p., John Wiley, Chichester.

Haque, M. I., and K. Mahmood (1985), Geometry of ripples and dunes, *J. Hydraul. Eng.*, *111*(1), 48–63.

Haque, M. I., and K. Mahmood (1986), Analytical study on steepness of ripples and dunes, *J. Hydraul. Eng.*, *112*(3), 220–236.

Haque, M. I., and K. Mahmood (1987), Sediment convection-diffusion and bedform length, *J. Hydraul. Eng.*, *113*(11), 1381–1401.

Hino, M. (1968), Equilibrium-range spectra of sand waves formed by flowing water, *J. Fluid Mech.*, *30*(3), 565–573.

Hoekstra, P., P. Bell, P. van Santen, N. Roode, F. Levoy, and R. Whitehouse (2004), Bedform migration and bedload transport on an intertidal shoal, *Cont. Shelf Res.*, *24*, 1249–1269.

Holmes, R. R. J., and M. H. Garcia (2008), Flow over bedforms in a large sand-bed river: A field investigation, *J. Hydraul. Res.*, *46*(3), 322–333.

Jackson, R. G. (1976), Largescale ripples of the lower wabash river, *Sedimentology*, *23*, 593–623.

Jacobson, R. B., and D. L. Galat (2006), Flow and form in rehabilitation of large-river ecosystems: An example from the lower Missouri River, *Geomorphology*, *77*, 249–269.

Jain, C. S., and J. F. Kennedy (1971), The growth of sand waves, in *International Symposium on Stochastic Hydraulics*, pp. 449–471, University of Pittsburgh School of Engineering Publication Series, Pittsburgh.

Jain, S. C., and J. F. Kennedy (1974), The spectral evolution of sedimentary bed forms, *J. Fluid Mech.*, *63*(2), 301–314.

Jerolmack, D., and D. Mohrig (2005), Interactions between bed forms: Topography, turbulence, and transport, *J. Geophys. Res.*, *110*, F02014, doi:10.1029/2004JF000126.

Jerolmack, D. J., D. Mohrig, and B. McElroy (2006), A unified description of ripples and dunes in rivers, in *River, Coastal and Estuarine Morphodynamics: RCEM 2005*, edited by G. Parker and M. H. Garcia, pp. 843–851, Taylor and Francis Group, London.

Julien, P. Y., and G. J. Klaasen (1995), Sand-dune geometry of large rivers during floods, *J. Hydraul. Eng.*, *121*(9), 657–663.

Julien, P. Y., G. J. Klaassen, W. B. M. T. Brinke, and A. W. E. Wilbers (2002), Case study: Bed resistance of Rhine River during 1998 flood, *J. Hydraul. Eng.*, *128*, 1042–1050.

Karbasi, M., M. H. Omid, and J. Farhoudi (2010), Experimental investigation of cluster bed-form formation over uniform sediment, *Am. J. Appl. Sci.*, *7*(8), 1093–1099.

Kaufmann, P. R., J. M. Faustini, D. P. Larsen, and M. A. Shirazi (2008), A roughness-corrected index of relative bed stability for regional stream surveys, *J. Geomorphology*, *99*, 150–170.

Kennedy, J. F. (1963), The mechanics of dunes and antidunes in erodible-bed channels, *J. Fluid Mech.*, *16*, 521–544.

Keylock, C. J., D. R. P. R. D. Hardy, R. I. Ferguson, S. N. Lane, and K. S. Richards (2005), The theoretical foundations and potential for large-eddy simulation (LES) in fluvial geomorphic and sedimentological research, *Earth-Sci. Rev.*, *71*, 271–304.

Kheiashy, K., J. McCorquodale, I. Georgiou, and E. Meselhe (2007), Geometric and statistical characteristics of bed forms in the lower Mississippi River, in *Sixth International Symposium on Coastal Engineering and Science of Coastal Sediment Process,* pp. 2,177–2,190, American Society of Civil Engineers, New Orleans, Louisiana, USA.

Kleinhans, M. (2004), Sorting in grain flows at the lee side of dunes, *Earth-Sci. Rev.*, *65*, 75–102.

Kleinhans, M. (2005), Grain-size sorting in grainflows at the lee side of deltas, *Sedimentology*, *52*(2), 291–311.

Knaapen, M. A. F. (2008), Local variation in the shape of superimposed bedforms as a function of local bathymetry, in *Proceedings of Marine Sandwave and River Dune Dynamics III*, School of Earth and Environment, University of Leeds.

Komarova, N., and A. Newell (2000), Nonlinear dynamics of sand banks and sand waves, *J. Fluid Mech.*, *415*, 285–321.

Kostaschuk, R. (2006), *Sediment transport mechanics and subaqueous dune morphology*, in *River Coastal and Estuarine Morphodynamics: RCEM 2005*, pp. 795–801, Taylor and Francis Group, London.

Kostaschuk, R. A., and M. A. Church (1993), Macroturbulence generated by dunes: Fraser River, Canada, *Sediment. Geol.*, *1-4*, 25–37.

Kroesse, D. P., T. Taimre, and Z. I. Botev (2011), *Handbook of Monte Carlo Methods*, Wiley and Sons Inc., USA.

Kuhnle, R. A., J. K. Horton, S. J. Bennett, and J. L. Best (2006), Bedforms in bimodal sand-gravel sediments: Laboratory and field analysis, *Sedimentology*, *40*, 631–654.

Kumar, B. (2011), Flow resistance in alluvial channel, *Hydrophysical Processes*, *38*(6), 745–754.

Kumar, P., and Foufoula-Georgiou (1993), A multicomponent decomposition of spatial rainfall fields. Segregation of large and small scale features using wavelet transforms, *Water Resour. Res.*, *29*, 2515–2532, doi:10.1029/93WR00549.

Labat, D. (2005), Recent advances in wavelet analyses: Part 1. A review of concepts, *J. Hydrol.*, *314*, 275–288.

Leclair, S. (2002), Preservation of cross-strata due to the migration of subaqueous dunes: An experimental investigation, *Sedimentology*, *49*, 1157–1180.

Leclair, S. F., J. S. Bridge, and F. Wang (1997), Preservation of cross-strata due to migration of subaqueous dunes over aggrading and non-aggrading beds: Comparison of experimental data with theory, *Geosci. Can.*, *24*, 55–66.

Levey, R. A., B. Kjerfve, and R. T. Getzen (1980), Comparison of bed form variance spectra within a meander bed during flood and average discharge, *J. Sediment. Petrol.*, *50*(1), 149–155.

Little, S. (1994), Wavelet analysis of seafloor bathymetry: An example, *Wavelets in Geophysics*, *4*, 167–182.

Liu, H.-K. (1957), Mechanics of sediment-ripple formation, *J. Hydraul. Div.*, *83*(2), 1–23.

Longhitano, S. G., and W. Nemec (2005), Statistical analysis of bed-thickness variation in a Tortonian succession of biocalcarenitic tidal dunes, Amantea Basin, Calabria, southern Italy, *Sediment. Geol.*, *179*, 195–224.

Maddux, T. B., S. R. McLean, and J. M. Nelson (2003), Turbulent flow over three-dimensional dunes: 2. Fluid and bed stresses, *J. Geophys. Res.*, *108*, 1–171, doi:10.1029/2003JF000018.

Mercer, A. J. (1971), Analytically determined bedform shape, *J. Eng. Mech. Div-Asce.*, *97*, 175–180.

Moll, J. R., T. Schilperoort, and A. J. De Leeuw (1987), Stochastic analysis of bedform dimensions, *J. Hydraul. Res.*, *25*(4), 465–479.

Morley, S. A., J. J. Duda, H. J. Coe, K. K. Kloehn, and M. L. McHenry (2008), Benthic invertebrates and periphyton in the Elwha River Basin: Current conditions and predicted response to dam removal, *Northwest Sci.*, *82*, 179–195.

Mostacci, E., C. Truntzer, H. Cardot, and P. Ducoroy (2010), Multivariate denoising methods combining wavelets and principal component analysis for mass spectrometry, *Proteomics*, *10*, 2564–2572.

Nikora, V. I., A. N. Sukhodolov, and P. M. Rowinski (1997), Statistical sand wave dynamics in one-directional water flows, *J. Fluid Mech.*, *351*, 17–39.

NIST/SEMATECH (2010), e-Handbook of Statistical Methods, NIST. http://www.itl.nist.gov/div898/handbook/.

Nordin, C. F., and J. H. Algert (1966), Spectral analysis of sand waves, *Proc. Am. Soc. Civil Engineers*, *92*, 95–114.

Nordin, C. F. J. (1971), *A stationary Gaussian model of sand waves*, in *International Symposium on Stochastic Hydraulics,* pp. 472–488, University of Pittsburgh School of Engineering Publication Series.

Nyander, A., P. S. Addison, I. McEwan, and G. Pender (2003), Analysis of river bed surface roughnesses using 2-D wavelet transform-based methods, *Arab. J. Sci. Eng.*, *28*(1C), 107–121.

Orfeo, O., and J. Stevaux (2002), Hydraulic and morphological characteristics of middle and upper reaches of the Paraná River (Argentina and Brazil), *Geomorphology*, *44*, 309–322.

Packman, A. I., M. Selehin, and M. Zaramella (2004), Hyporheic exchange with gravel bed: Basic hydrodynamic interactions and bedform-induced advective flows, *J. Hydraul. Eng.*, *130*(7), 647–656.

Paola, C., and L. Borgman (1991), Reconstructing random topography from preserved stratification, *Sedimentology*, *38*, 553–565.

Parsons, D. R., J. L. Best, O. Orfeo, R. J. Hardy, R. Kostaschuk, and S. N. Lane (2005), Morphology and flow fields of three-dimensional dunes, Rio Parana, Argentina: Results from simultaneous multibeam echo sounding and acoustic Doppler current profiling, *J. Geophys. Res.*, *110*, doi:10.1029/2004JF000231.

Prave, A. R., and W. L. Duke (1990), Small-scale hummocky cross-stratification in turbidites: A form of antidune stratification? *Sedimentology*, *37*, 531–539.

Prent, M. T. H., and E. J. Hickin (2002), Annual regime of bedforms, roughness and flow resistance, Lillooet River, British Columbia, BC, *Geomorphology*, *41*, 369–390.

Prokoph, A., and J. Veizer (1999), Trends, cycles and nonstationarities in isotope signals of phanerozoic seawater, *Chem. Geol.*, *161*, 225–240.

Quin, J. G. (2011), Is most hummocky cross-stratification formed by large-scale ripples? *Sedimentology*, *58*, 1414–1433.

Raja, J., B. Muralikrishnan, and S. Fu (2002), Recent advances in separation of roughness, waviness and form, *Precis. Eng.*, *26*, 222–235.

Raudkivi, A. J. (1997), Ripples on stream bed, *J. Hydraul. Res.*, *123*(1), 58–64.

Reesink, A. J. H., and J. S. Bridge (2011), Evidence of bedform superimposition and flow unsteadiness in unit-bar deposits, South Saskatchewan River, Canada, *J. Sediment. Res.*, *81*, 814–840, doi:10.2110/jsr.2011.69.

Richards, K. J. (1980), The formation of ripples and dunes on an erodible bed, *J. Hydraul. Res.*, *99*, 597–618.

Robert, A., and W. Uhlman (2001), An experimental study on the ripple-dune transition, *Earth Surf. Processes Landforms*, *26*, 615–629.

Rossi, A., N. Massei, B. Laignel, D. Sebag, and Y. Copard (2009), The response of the Mississippi River to climate fluctuations and reservoir construction as indicated by wavelet analysis of streamflow and suspended-sediment load, 1950–1975, *Journal of Hydrology*, *377*(3-4), 237–244.

Shugar, D. H., R. Kostaschuk, J. L. Best, D. R. Parsons, S. N. Lane, O. Orfeo, and R. J. Hardy (2010), On the relationship between flow and suspended sediment transport over the crest of a sand dune, Río Paraná, Argentina, *Sedimentology*, *57*, 252–272.

Simons, D. B., and E. V. Richardson (1962), *The Effect of Bed Roughness on Depth Discharge Relations in Alluvial Channels (Studies of Flow in Alluvial Channels)*, 26 p., U.S. Geological Survey, Washington, USA.

Singh, A., K. Fienberg, D. J. Jerolmack, J. Marr, and E. Foufoula-Georgiou (2009), Experimental evidence for statistical scaling and intermittent in sediment transport rates, *J. Geophys. Res.*, *114*, doi:10.1029/2007JF000963.

Singh, A., S. Lanzoni, P. R. Wilcock, and E. Foufoula-Georgiou (2011), Multiscale statistical characterization of migrating bed forms in gravel and sand bed rivers, *Water Resour. Res.*, *47*, W12526, doi:10.1029/2010WR010122.

Stoesser, T., C. Braun, M. García-Villalba, and W. Rodi (2008), Turbulence structures in flow over two-dimensional dunes, *J. Hydraul. Eng.*, *134*, 42–55.

Storms, J. E. A., R. L. van Dam, and S. F. Leclair (1999), Preservation of cross-sets due to migration of current ripples over aggrading and non-aggrading beds: Comparison of experimental data with theory, *Sedimentology*, *46*, 189–200.

Takeda, A. M., J. Stevaux, and D. S. Fujita (2001), Effect of hydraulics, bedload grain size and water factors on habitat and abundance of Narapa bonettoi Righi and Varela, 1983 of the upper Parana River, Brazil, *Hydrobiologia*, *463*, 241–248.

Takezawa, K. (2006), *Introduction to Nonparametric Regression*, 640 p., John Wiley and Sons, New Jersey, USA.

Torrence, C., and G. P. Compo (1998), A practical guide to wavelet analysis, *B. Am. Meteorol. Soc.*, *79*, 61–78.

Tuijnder, A. P., and J. S. Ribberink, (2009), Prediction of bedform dimensions, bed roughness and sediment transport under supply-limited conditions in rivers, *Tech. rep.*, Faculty of Engineering Technology, University of Twente, The Netherlands.

van der Mark, C. F., and A. Blom (2007), A new and widely applicable bedform tracking tool, *Tech. rep.*, University of Twente, Faculty of Engineering Technology, Department of Water Engineering and Management.

van der Mark, C. F., A. Blom, J. M. H. Hulscher, S. F. Leclair, and D. Mohrig (2006), On modeling the variability of bedform dimensions, in *River, Coastal and Estuarine Morphodynamics: RCEM 2005*, edited by G. Parker and M. H. García, pp. 831–841, Taylor and Francis Group, London.

van der Mark, C. F., A. Blom, and J. M. H. Hulscher (2008a), Variability of bedform characteristics using flume and river data, in *River, Coastal and Estuarine Morphodynamics: RCEM 2007*, edited by C. M. Dohmen-Janssen, and S. J. M. H. Hulscher, pp. 923–930, Taylor and Francis Group, London.

van der Mark, C. F., A. Blom, and J. S. M. Hulscher (2008b), Quantification of variability in bedform geometry, *J. Geophys. Res.*, *113*, doi:10.1029/2007JF000940.

Venditti, J. G. (2007), Turbulent flow and drag over fixed two- and three-dimensional dunes, *J. Geophys. Res.*, *112*, 1–21, doi:10.1029/2006JF000650.

Venditti, J. G., M. Church, and S. J. Bennett (2005), On the transition between 2D and 3D dunes, *Sedimentology*, *52*, 1343–1359.

Wang, Z.-Q., and N.-S. Cheng (2006), Time-mean structure of secondary flows in open channel with longitudinal bedforms, *Adv. Water Resour.*, *29*, 1634–1649.

Warmink, J. J., M. J. Booij, S. J. M. H. Hulscher, and H. V. der Klis (2010), Uncertainty in design water levels due to uncertain bed form roughness in the River Rhine, in *International Conference on Fluvial Hydraulics (River Flow 2010)*, IAHR - Fluvial Hydraulics Committee, Technische Universität Braunschweig, EWE Aktiengesellschaft, Braunschweig, Germany, 359–366.

Wilbers, A. W. E., and W. B. M. T. Brinke (2003), The response of subaqueous dunes to floods in sand and gravel bed reaches of the dune rhine, *Sedimentology*, *50*, 1013–1034.

Wildhaber, M. L., P. J. Lamberson, and D. L. Galat (2003), A comparison of measures of riverbed form for evaluating distributions of benthic fishes, *N. Am. J. Fish. Manage.*, *23*, 543–557.

Yalin, M. S. (1964), Geometrical properties of sand waves, *J. Hydr. Eng. Div.*, *90*, 105–119.

Yalin, S., and G. Lai, (1985), On the form drag caused by sand waves, *Tech. Rep. 363/II-4*, Japan Society of Civil Engineers.

Yang, S.-Q., S.-K. Tan, and S.-Y. Lim (2005), Flow resistance and bed form geometry in a wide alluvial channel, *Water Resour. Res.*, *41*, doi:10.1029/2005WR004211.